École Polytechnique Fédérale de Lausanne
Haute école du paysage, d'ingénierie et d'architecture de Genève

Semester Project Report

AVONI Leonardo; N.Sciper:301524

EPFL-HEPIA professor: Flavio Noca

Supersonic wind tunnel for Space

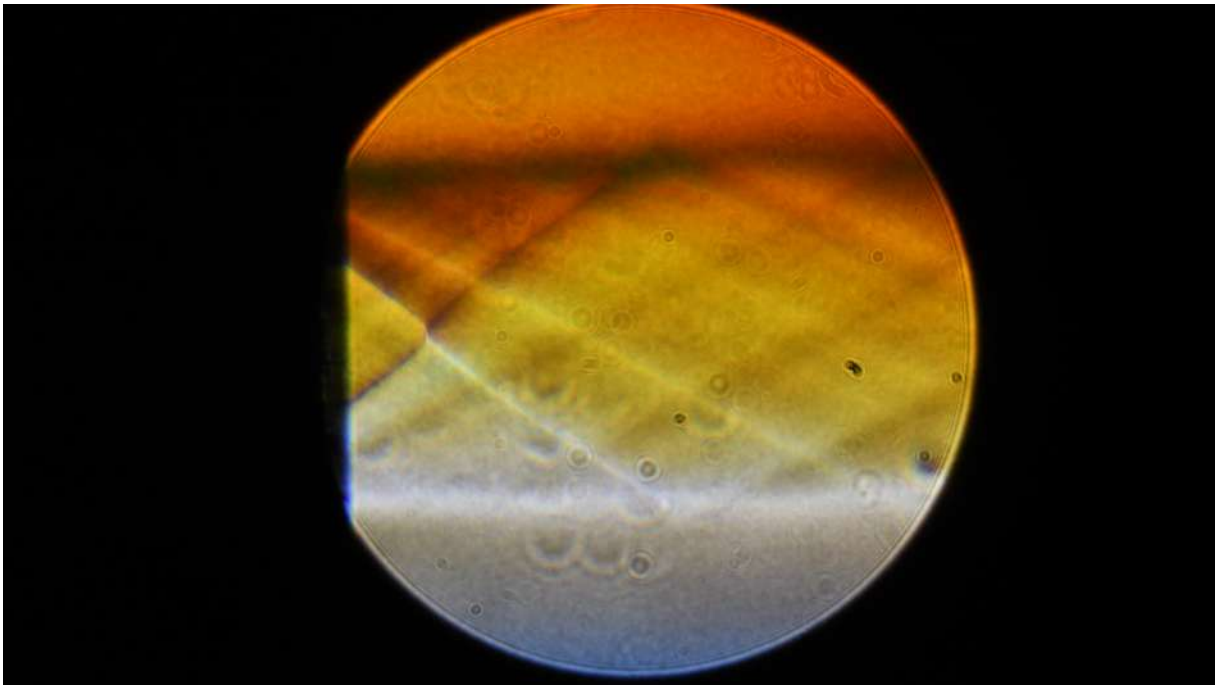

Figure 1: Image of the flow obtained on the back of a nozzle designed for Mach 2.2 (characteristics method, throat diameter of 2mm). The reservoir pressure is 8 bar (relative pressure); the flow is close to the nominal regime. Mach waves are present.

April 26, 2026

Table of contents

1 Introduction **2**
- 1.1 Quick literature review / state of the art . . . 2
  - 1.1.1 Literature about wind tunnels . . . 2
  - 1.1.2 Studies about compressible flows . . . 2
  - 1.1.3 Numerical flow simulations . . . 2
- 1.2 Current available hardware . . . 2
- 1.3 Planning of this project . . . 3
- 1.4 Timeline of the project . . . 4

2 The previous wind tunnel assembly **4**

3 Initial studies on the available hardware **5**
- 3.1 Introduction . . . 5
- 3.2 Progressive nozzles mass flow rate test system . . . 6

4 Practical build **10**
- 4.1 The wind tunnel . . . 10
- 4.2 The nozzles . . . 13
- 4.3 The Schlieren observation system . . . 14
  - 4.3.1 The Schlieren and Shadowgraphy visualization techniques . . . 14
  - 4.3.2 The Schlieren alignment procedure . . . 15
  - 4.3.3 The Schlieren focus problem . . . 16
- 4.4 Example image . . . 17
  - 4.4.1 List of components . . . 18

5 The various experimentations **19**
- 5.1 Experimentation 1 . . . 19
- 5.2 Experimentation 2 . . . 20
- 5.3 Experimentation 3 . . . 23
- 5.4 Experimentation 4 and 5 . . . 24
- 5.5 Experimentation 6 . . . 26
- 5.6 Experimentation 7 . . . 26
- 5.7 Practical problems . . . 27
- 5.8 Nozzle measurements . . . 27
- 5.9 Conclusion of the experiments . . . 29

6 CFD study **29**
- 6.1 Simulation 1 . . . 29

7 Conclusion and further works **32**

Abstract

1 Introduction

Wind tunnels are infrastructures meant to provide a fluid flow at a certain speed, in order to be able to test certain geometries, often at reduced scale, in order to check the flow behaviour. Checking the aerodynamics performance of objects is important not only for aeronautical reasons (drone and aircraft testings), but also for space applications (testings of reentry shields undergoing supersonic/hypersonic flows). CFD alone does not necessarily provide the same results because of various reasons, such as simplifications (inviscid flow, laminar flow, viscous models...), meshing resolution (the results are only as spatially precise as the local mesh size, and also depending on the meshing size, the results are more or less accurate with reality[1]), solver methods, and many other numerical problems, [7]. In general, what is done is CFD, with real testings, in order to validate the CFD [7]. In this project, carried over in collaboration with Pietro DAVI, the initial goal was to build a wind tunnel able to reach Mach 2.2 with compressed air, and adapt a Schlieren system in order to observe the flow. Additional goals included, but were not limited to:

- Using multiple gases (CO2, Nitrogen, Helium) instead of air
- Making a closed-loop tunnel
- Developing a tunnel for various Mach numbers

1.1 Quick literature review / state of the art

1.1.1 Literature about wind tunnels

Wind tunnels are mainly divided in two categories: open wind tunnels [8], and closed wind tunnels [3]. More details on the working principles, advantages/disadvantages... of the two types can be obtained from [12]. For our case, the main motivation behind the initial selection of an open wind tunnel (blowdown) is its simplicity. Examples of supersonic setups have been produced, for example [11], from which we will take inspiration.

1.1.2 Studies about compressible flows

In order to analyse the flow beyond Mach 0.3, we are needed to understand compressible flow dynamics, detailed in the course ME-343 at EPFL (Compressible-fluid dynamics by Flavio Noca, [4]). The course details the main laws to use for the following scenario: inviscid and isentropic flow (except for chock-waves) of perfect gases. To study the flow inside a nozzle, the theory also assumes unidirectional flow. After developments, detailed in the course, laws and formulas can be deduced, that help to obtain the characteristics of the flow (pressure, temperature, Mach number...) depending on the shape of the nozzle used. Note that for this report, the nomenclature exposed in the Compressible-fluid dynamics course [4] will be used (M,γ,A_*,a,...). Also, when using the equations from the course, we will assume the same hypothesis used in the course (quasi-unidirectional flow, isentropic, constant properties, perfect gas). An exception will be made when studying characteristics-method flow (not unidirectional).

1.1.3 Numerical flow simulations

Concerning the potential numerical flow simulations (CFD) that can be done for this project, those will be carried out using Ansys Fluent [1], following the theory explained in the EPFL course "Numerical Flow Simulation" [7].

1.2 Current available hardware

The available initial hardware consists of the following:

- A JAG 7-270E compressor from Volkart [9]. The compressor has the following specifications:
  - Power: 7.5 kW
  - Volume flow rate (8 bar pressure): 1100 L/min
  - Volume flow rate (10 bar pressure): 950 L/min
  - Volume flow rate (13 bar pressure): 750 L/min

[1] This part can be improved doing a convergence study

  - Reservoir: 270 L
  - Provided with air water remover (primary filter: 0.1 μm, secondary filter: 0.01 μm)
- A worktable with various assemblies, previously used with a small supersonic De Laval nozzle pointing downwards
- A Schlieren assembly, made to observe the flow from the vertical nozzle
- additional 12.5mm, 25mm and 50mm lenses for the Schlieren assembly
- 200 bar bottles of CO2, Nitrogen and Helium
- various connectors, and various expander valves

The various hardware is shown in Figure 2.

Figure 2: Hardware initially provided for the project. The JAG-7 270E is shown in the center, while the wind tunnel hardware is displayed on the table

1.3 Planning of this project

After discussing with both Flavio Noca, and Pietro Davi, a planning for the operations to perform has been established:

1. Review of litterature concerning wind tunnels and compressible flows (ME-343 course from EPFL)
2. Theoretical and practical studies about the real maximum achievable flow rate of the compressor
3. Theoretical design of an open wind tunnel, designed for Mach 2.2, and working with Air
    - The tunnel would only consist of a properly designed de Laval nozzle, followed by the test section, and nothing else. The gas will hence deverse in athmosphere

4. Practical assembly of the Mach 2.2 wind tunnel, also including the test section and the Schlieren assembly to observe the flow
5. Designing additional wind tunnels for various mach numbers and/or various gases
6. Practical assembly of the various wind tunnels for various mach numbers and/or various gases
7. If everything is ok so far, trying to study a closed-loop tunnel (this part is complicated because of the addition of various components, like cooler and nozzle heater)

1.4 Timeline of the project

A Gantt chart of the project is shown in Figure 3.

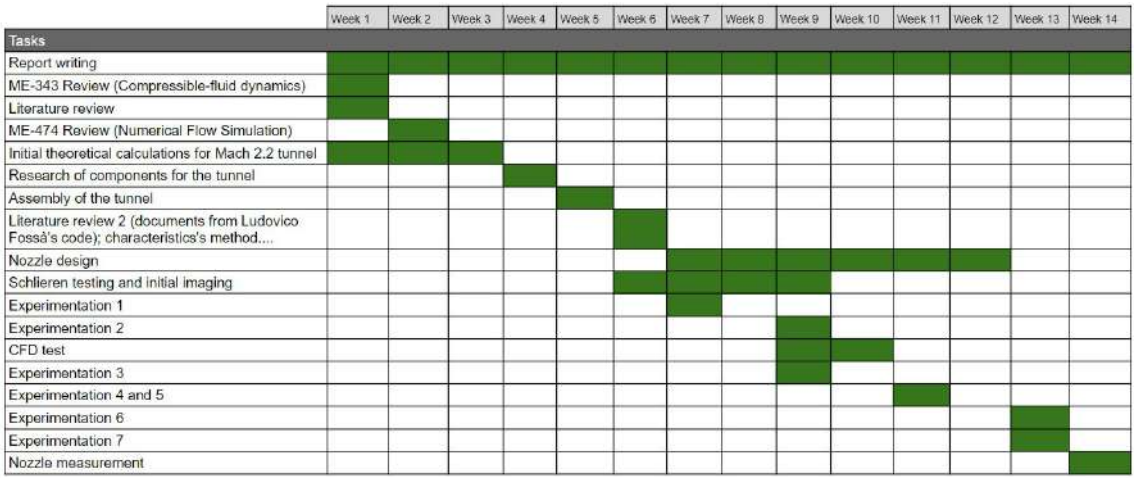

Figure 3: Gantt chart of the project, describing the tasks accomplished by Leonardo AVONI. The tasks from Pietro Davi are not shown.

2 The previous wind tunnel assembly

Before our begin of the project, a previous wind tunnel, with Schlieren assembly was already in place. Such system is able to create a supersonic jet (Mach approx. 1.7, a few mm diameter) using the compressed air grid of HEPIA. The system is shown in Figure 4

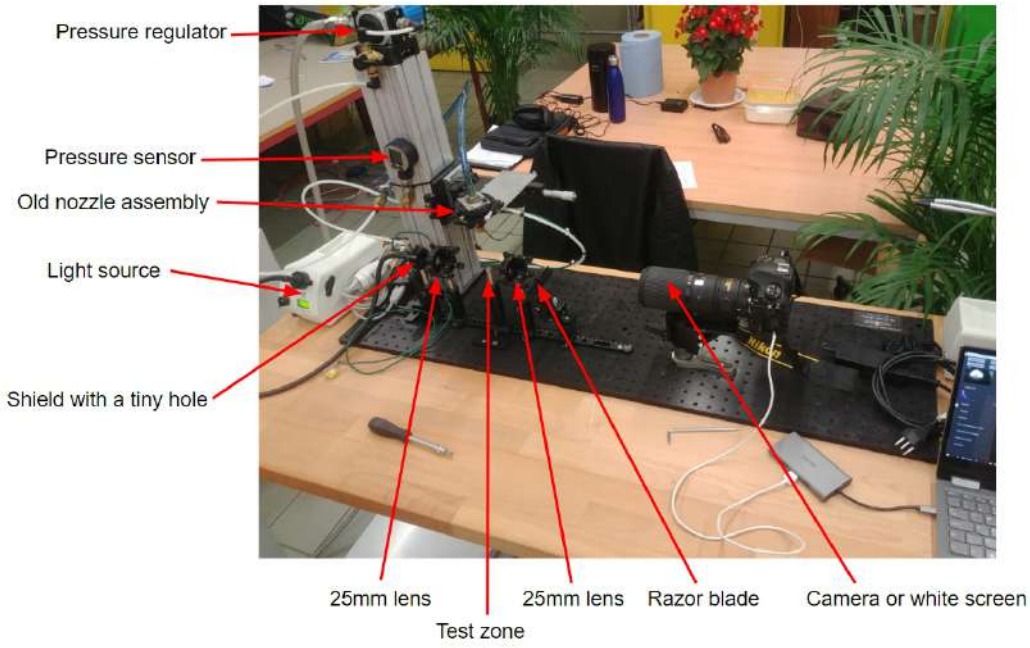

Figure 4: Initial assembly provided for the project

Such wind tunnel assembly should not be dismantled, since it will be used for classroom display, still, we could take inspiration from it. Note that throughout the whole project, we relied on the Schlieren assembly from this bench.

3 Initial studies on the available hardware

3.1 Introduction

The nomenclature from the Compressible-Fluid dynamics [4] will be used. All the formulas used, if not specified otherwise, have been obtained in that course.

For this project, it is implicit that one goal is to maximize the test area dimensions as much as possible. From the course, the ratio A_{out}/A_* is dictated by a law of the number of Mach needed at the end of the nozzle (thus is fixed). Meaning that the goal, in order to have a test section as big as possible, is to have the biggest possible A_*. However, we know that the mass flow rate $\dot{m}$ is given by (as long as we have sonic blockage)

$$\dot{m} = f(\gamma)\frac{P_0 A_*}{\sqrt{RT_0}} \tag{1}$$

and is thus proportional to A_*. This means that the bigger the test section, the bigger the mass flow rate.

We also know that the compressor, but very probably also the 200 bar bottles + expander valves probably have a limit in the maximum mass flow rate they are allowed to deliver. In order to be 100% sure of what this limit is (before designing an actual tunnel), we decide to develop a system that would allow us to test the upstream assembly for bigger and bigger mass flow rates, until the upstream assembly is no longer able to provide bigger flows, and the outled becomes subsonic suddenly.

To do so, it is crucial to understand under what conditions a de Laval nozzle works. From [4], there is a minimum reservoir pressure that allows to have sonic blockage (sonic flow at the throat of the nozzle). In theory, by increasing the reservoir pressure from the athmospheric pressure, we reach three scenarios:

- $P_{reservoir} = P_{shockwaves,throat}$
- $P_{reservoir} = P_{shockwaves,outlet}$
- $P_{reservoir} = P_{0,max}$ (maximum pressure delivered by the upstream component)

The idea will be to design first one nozzle, that goes from $P_{shockwaves,outlet}$, to $P_{0,max}$ (with a mass flow rate that ranges linearly from the two pressure values, based on Equation 1). Once we reach the maximum allowable pressure $P_{0,max}$, if we need to increase more the mass flow rate because we did not reach the limit point of the mass flow rate

of the upstream components, we can change the nozzle for a bigger one, made such that the minimum flow (obtained for $P = P_{shockwaves,outlet}$) is equal to the one reached by the previous nozzle when the pressure was $P = P_{0,max}$. In order to detail better the procedure, we will show the math used:

3.2 Progressive nozzles mass flow rate test system

Before detailing the math, we will explain what is expected when placing a De Laval nozzle after a pressurized reservoir/compressor (we will refer to those points later):

1. The reservoir pressure will initally be at P_{atm}; then will be raised
2. At a certain point, sonic conditins will appear at the throat, but with a shock wave just afterwards since the reservoir pressure is still too small
3. Raising the reservoir pressure will lead to the movement of the shock wave from the throat to the exit of the nozzle
4. Raising again the pressure will generate oblique shock waves, and diamond-shaped systems at the end of the nozzle
5. Raising again the pressure will lead after a certain point to the optimal scenario (exit pressure at the nozzle is equal to the athmosperic pressure)
6. Raising again the pressure will result in Prandtl-Meyer fans appearing directly at the end of the nozzle
7. At a certain point, raising more the pressure will not be possible, because we will have reached the limit for the upstream reservoir, with respect to the possible mass flow rate, thus the pressure will either stay constant, or decrease. Another scenario is that we reach the maximum possible pressure deliverabe by the reservoir, thus, if we want to continue with bigger flow rates, we will be forced to use a bigger nozzle

For more details, the behaviour of the nozzle, with respect to the reservoir pressure can also be seen in Figure 23. Now that we understand the main idea of the system, we can proceed with the math. In order to develop the system composed of a series of nozzles, we decide to remind the main equations to use. Equation 2[2] describes the mass flow rate in a De Laval nozzle, assuming that sonic blockage happened at the throat of the nozzle.

$$\dot{m} = \sqrt{\gamma}\left(\frac{\gamma+1}{2}\right)^{-\frac{\gamma+1}{2(\gamma-1)}} \frac{P_0 A_*}{\sqrt{rT_0}} \tag{2}$$

Equation 3 links the Mach number with the area ratio, inside a de Laval nozzle (assuming no shock waves inside the nozzle)

$$\frac{A}{A_*} = \frac{1}{M}\left[\frac{2}{\gamma+1}\left(1+\frac{\gamma-1}{2}M^2\right)\right]^{\frac{\gamma+1}{2(\gamma-1)}} \tag{3}$$

Equation 4 links the reservoir pressure, with the pressure at a certain point having a certain Mach number (assuming isentropic expansion).

$$\frac{P_0}{P} = \left(1+\frac{\gamma-1}{2}M^2\right)^{\frac{\gamma}{\gamma-1}} \tag{4}$$

When going through a straight shock wave, we have the following relationship between the upstream and the downstream pressure, depending on the Mach number before the shock waves (Equation 5):

$$\frac{P_{atm}}{P} = 1 + \frac{2\gamma}{\gamma+1}\left(M^2-1\right) \tag{5}$$

In order to perform the math, we will define the following parameters:

- Required Mach number at the exit of the nozzle M_{out}
- $\gamma = \frac{C_p}{C_v}$
- R ideal gas constant

[2]Like equation 1, but with the $f(\gamma)$ term explicited

- P_{atm}
- $P_{0,max}$ (maximum reservoir pressure)
- T_0 reservoir temperature

Now, proceeding to the math for the different points listed previously:

1. No math is needed, since no studies on the subsonic regime are performed
2. For that condition, we will assume a shock wave at the throat of the nozzle (relationship between the pressures on the two sides of the wave using Equation 5, for M=1), then relationship between the reservoir pressure and the pressure upstream the wave (Equation 4)
3. For that, we will consider the case where the shock waves is located at the exit of the nozze (pressure difference with the athmospheric pressure ruled by Equation 5, with the Mach number defined by Equation 3 or fixed by our needs), then will use Equation 4 in order to obtain the reservoir pressure. In order to reach 3. from 2., the pressure has to be increased monotonically. Once at 3., the pressure will be able to increase after the shock wave, in order to reach the atmospheric pressure
4. Raising again the pressure will result in a back pressure before the shock wave between the atmospheric pressure and the pressure obtained at 3. A pressure in between will result naturally in oblique shock waves.
5. We can obtain the reservoir pressure needed in that case simply by removing the shock waves in case 3.
6. Just increase the pressure
7. Trivial

Note: Going from 2. to 3. is possible by increasing the reservoir pressure. This can be understood by supposing a shock waves in the diverging part of the nozzle (at a certain mach number). By doing so, we can relate the outer athmospheric pressure P_{atm} with the pressure upstream the shock waves (Equation 5), then relate the Reservoir pressure with the pressure just upstream the shock waves (Equation 4). This way, we can express $\frac{P_0}{P_{atm}} = f(M)$, and this function turns out to be strictly increasing. Thus, increasing the reservoir pressure will cause a need for a bigger Mach number, and so under Equation 3, it will cause the shock waves to move to the exit of the de Laval nozzle.

By doing all the math, and showing it on a graph, we are able to obtain what is shown in Figure 5. Such graph has been obtained using the following data:

- $M_{out} = 2.2$
- $\gamma = 1.4$
- $R = 287 J/kg/\check{r}K$
- $P_{atm} = 101325$ Pa
- $P_{0,max} = 13$ Bar
- $T_0 = 300$ °K
- $d_{throat,1} = 1$ mm (First nozzle's throat diameter)
- $d_{throat,2} = 2.5642$ mm
- $d_{throat,3} = 6.5754$ mm
- $d_{throat,4} = 16.8608$ mm
- $d_{throat,5} = 43.2353$ mm

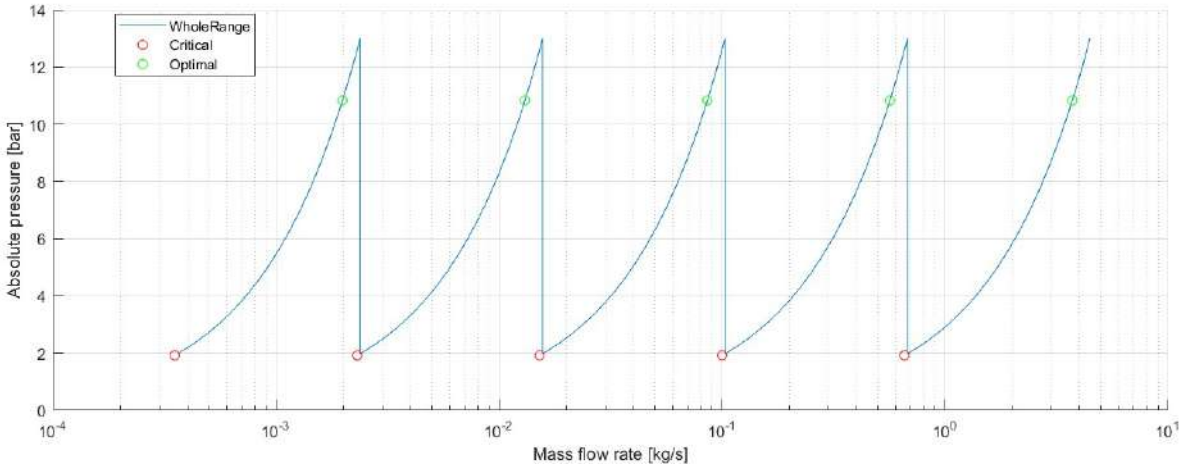

Figure 5: Pressure to mass flow rate achieved, for various nozzles. We used the parameters detailed previously. We note the operation range for each nozzle, as well as the point where a shock wave appears at the throat (red circles), and the optimal point, where there are no shock waves, nor PM fans (green circles).

- Note that the flow is only useful after the optimal point (before, the flow speed is smaller than Mach 2.2)
- Note that we did not pay particular attention to the shape of the nozzle, we instead supposed the flow unidirectional and relied only on the ratio of the areas
- Gamma=1.4 for air, 5/3 for He, Ar,
- Assumed constant properties, constant reservoir properties

The code used to produce the graph is the following:

```
1
2  clear,clc,close all;
3
4  M_out=2.2;
5  gamma=1.4;
6  r=287; %J/kg/ K
7  P_atm=101325; %Pa
8  Rapport_gamma=sqrt(gamma)*((gamma+1)/2)^(-(gamma+1)/(2*gamma-2));
9  P_0_max=13*10^5;
10 T_0=273+60; % K
11
12 %throat dimensions
13 d_start=2.5; %mm
14 d_start=d_start*0.001;
15 Area_star=pi*d_start^2/4;
16
17 %%
18 P_out=P_atm/(1+(2*gamma)*(M_out^2-1)/(gamma+1));
19
20 P_0_min=P_out*(1+(gamma-1)*0.5*M_out^2)^(gamma/(gamma-1));
21
22 Area_ratio=(1/M_out)*((2/(gamma+1))*(1+(gamma-1)*0.5*M_out^2))^((gamma+1)/(2*gamma-2));
23
24 m_dot_min=Rapport_gamma*P_0_min*Area_star/(sqrt(r*T_0));
25 m_dot_max=Rapport_gamma*P_0_max*Area_star/(sqrt(r*T_0));
26
27 P_0_critical=P_atm*((gamma+1)/2)^(gamma/(gamma-1));
28 m_dot_critical=Rapport_gamma*P_0_critical*Area_star/(sqrt(r*T_0));
29
30 P_0_optimal=P_atm*(1+(gamma-1)*0.5*M_out^2)^(gamma/(gamma-1));
31 m_dot_optimal=Rapport_gamma*P_0_optimal*Area_star/(sqrt(r*T_0));
32
33 Area_out=Area_ratio*Area_star;
34
```

```
[lin_pressure,lin_massflowrate]=Interpol(P_0_min,P_0_max,m_dot_min,m_dot_max,100);

%%
%{
We will create 4 vectors:
Area_star: defining the throat area of each nozzle
Area_out: difining the outlet area of each nozzle
m_dot_min: defining the minimum mass flow
m_dot_max: defining the maximum mass flow
m_dot_critical: defining the minimum mass flow, is chockwave at throat
m_dot_optimal: mass flow rate as if the nozzle was optimal
%}

%% Iteration
N=5;
for n=2:N
    Area_star(n)=m_dot_max(n-1)*sqrt(r*T_0)/(Rapport_gamma*P_0_min);
    Area_out(n)=Area_ratio*Area_star(n);
    m_dot_min(n)=m_dot_max(n-1);
    m_dot_max(n)=Rapport_gamma*P_0_max*Area_star(n)/(sqrt(r*T_0));
    m_dot_critical(n)=Rapport_gamma*P_0_critical*Area_star(n)/(sqrt(r*T_0));
    m_dot_optimal(n)=Rapport_gamma*P_0_optimal*Area_star(n)/(sqrt(r*T_0));

    [p,m]=Interpol(P_0_min,P_0_max,m_dot_min(end),m_dot_max(end),100);
    lin_pressure=[lin_pressure,p];
    lin_massflowrate=[lin_massflowrate,m];
    clear p m

end
d_star=sqrt(Area_star*4/pi)*1000; %mm
d_out=sqrt(Area_out*4/pi)*1000; %mm


%%
%Min_p_data=P_0_min*ones(1,N);
%Max_p_data=P_0_max*ones(1,N);
%Pressure_data=reshape([Min_p_data;Max_p_data],[1,2*N]);



%Flow_data=reshape([m_dot_min;m_dot_max],[1,2*N]);

%% Plotting stuff
figure(1)
    hold on
    xlabel("N. Nozzle [#]")
    ylabel("Diameter [mm]")
    scatter(1:N,d_star,"DisplayName","Throat")
    scatter(1:N,d_out,"DisplayName","Out")
    set(gca, 'YScale', 'log')
    grid on
    legend

figure(2)
    hold on
    xlabel("Mass flow rate [kg/s]")
    ylabel("Absolute pressure [bar]")
    plot(lin_massflowrate,lin_pressure*10^(-5),"DisplayName","WholeRange")
    scatter(m_dot_critical,P_0_critical*ones(1,N)*10^(-5),"red","DisplayName","Critical")
    scatter(m_dot_optimal,P_0_optimal*ones(1,N)*10^(-5),"green","DisplayName","Optimal")
    grid on
    set(gca, 'XScale', 'log')
    legend
    hold off
%% Bonus math for chockwave in the de Laval nozzle
%{
M_out=linspace(1,10,1000);
gamma=1.4;
P0_Patm=((1+(gamma-1)*0.5.*M_out.^2).^(gamma/(gamma-1))./(1+(2*gamma/(gamma+1))*(M_out.^2-1));
figure(3)
plot(M_out,P0_Patm)
%}
```

```
%% FUNCTIONS

function [lin_pressure,lin_massflowrate]=Interpol(Pmin,Pmax,m_min,m_max,N)
    percent=linspace(0,1,N);
    lin_pressure=Pmin+(Pmax-Pmin).*percent;
    lin_massflowrate=m_min+(m_max-m_min).*percent;
end
```

We can also pay more attention to the shape of the divergent part of the de Laval nozzle, by using a code that implements the characteristic method (see [4]), thus optimizes the supersonic behaviour of the nozzle. Such code is obtained from [2]. We can also create a converging profile as smooth as possible (no abrupt change of area). If we do so, we can obtain the nozzle shown in Figure 6

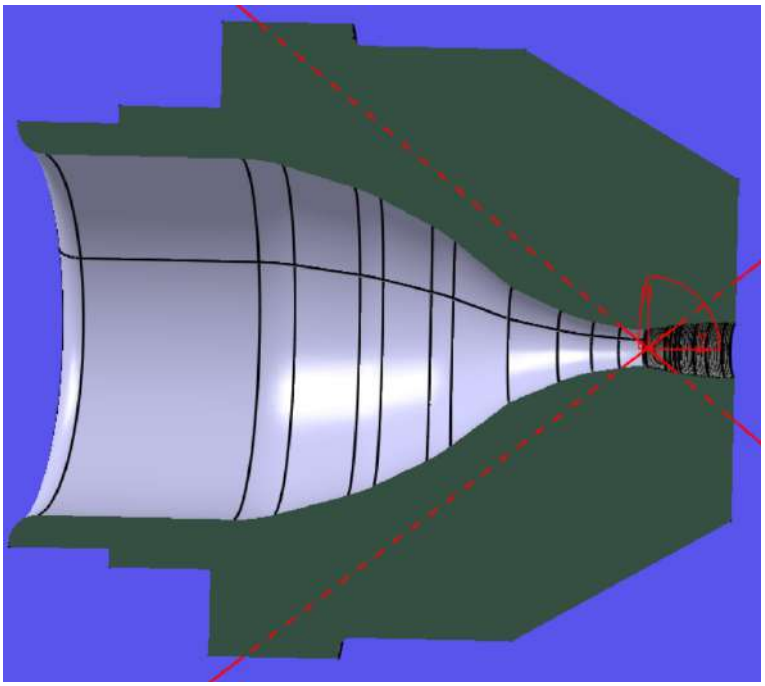

Figure 6: Cross-cut of the first nozzle created. The converging part was done manually, while a code has been used for the generation of the diverging side. The throat diameter is 2.5mm this time. This choice is explained in Section 4

When using such nozzle, generated using the characteristic's method, the previous math based on the area ratio is no longer 100% valid (the flow is no longer unidirectional). However, the general behaviour of the nozzle is the same. The only main difference is that the outer diameter of the nozzle is slightly different than the one predicted with A_{out}/A_*.

4 Practical build

4.1 The wind tunnel

This section details the practical assembly of the wind tunnel. The main guideline that has been followed is to keep the cross-sectional area of the various tubings used as large as possible (in order to be able to use a bigger nozzle, without having sonic blockage anywhere else than the nozzle). For the wind tunnel, we also installed instrumentation. In theory, in order to have all the characteristics of the flow, we would need the static pressure, total pressure and total temperature. However, measuring the total pressure can be tricky due to the need to position a pitot tube precisely inside the wind tunnel. Thus we decided to install the following instruments:

- A thermocouple, on the surface of the tubings, in order to measure the total temperature of the fluid in the subsonic region. the thermocouple would be insulated from the external environment. Positionning the thermocouple inside the tube would have been more complicated
- A pressure sensor, measuring the static pressure inside the wind tunnel, in the subsonic region [5]

- A flowmeter, able to measure pressure, temperature, volume flow rate and other parameters in the subsonic region of the wind tunnel [6]

The tunnel, built using 1" tubing is shown (without the instruments) in Figure 7

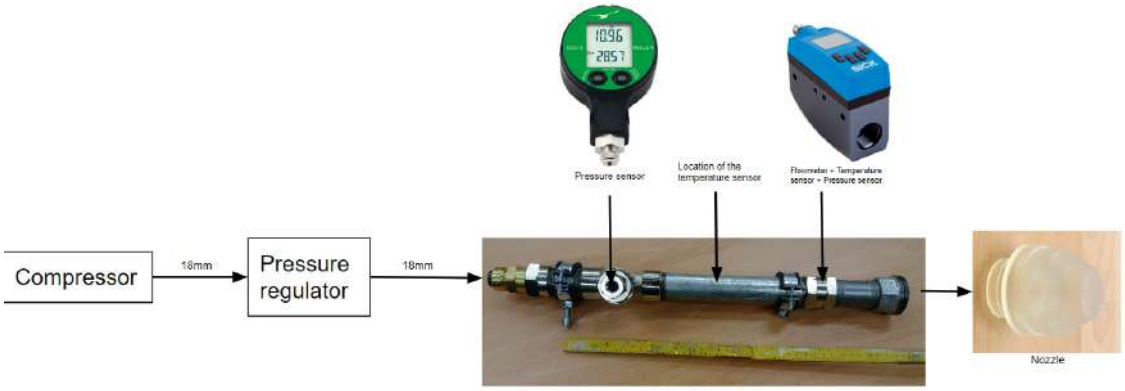

Figure 7: Wind tunnel, assembled in a temporary way, without any sensor installed. The hardware was purchased at Volkart SA

Concerning the static pressure sensor, we decided to install it using a metal T. In order to reduce turbulence inside the tunnel due to the presence of the T, we installed a plastic cap, making the inside of the T similar to a smooth tube, except for a small hole (needed to convey the pressure information). The cap was fixed in place using 15-minutes epoxy. The hardware is shown in Figure 8.

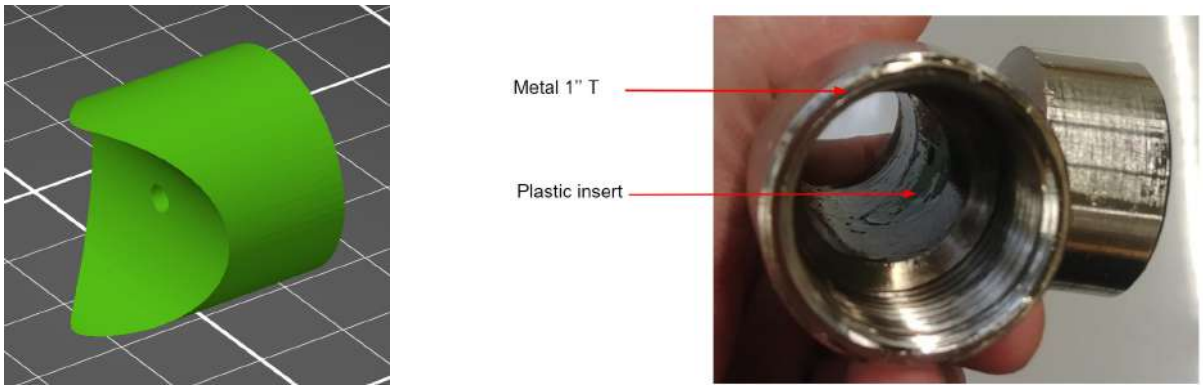

Figure 8: The left image shows the CAD of the cap, that has been 3D-printed, then installed inside the 1" T, shown on the right. As can be seen, the T is smooth, thus improving the quality of the measurements obtained with the tunnel, as well as the quality of the flow.

The nozzle producing the supersonic flow was designed using a characteristic method code (diverging part). The nozzle has been SLA-3D printed (better smoothness, especially at the throat compared to FDM). The nozzle and its fixation is shown in Figure 9

Figure 9: On the left image, the fixation (commonly used in plumbing) is shown. One element of the fixation was redesigned to be the nozzle, leading to the design on the right

In order to support the wind tunnel, a support has been built using aluminium profiles. Such assembly is shown in Figure 10

Figure 10: Support for the wind tunnel. The support is very rudimental. Still, it allows regulation of height due to the sliding grooves on the profile

The support is meant to be clamped to the test table during use; still, it was found that even at maximum pressure, low reaction force was generated by the systems, making clamps unnecessary. Anyway, clamping is preferred for safety reasons.

Of course, better alternatives involving the use of micrometric rail systems, probably offered by Thorlabs are possible. Still, the idea was to first test the nozzle system and the visualization system (Schlieren) before proceeding further. One possible alternative has been developed by Pietro Davi (better explained in his report), consisting in a set of sliding joints, allowing precise adjustments of the position of the jet. The solution is shown in Figure 11

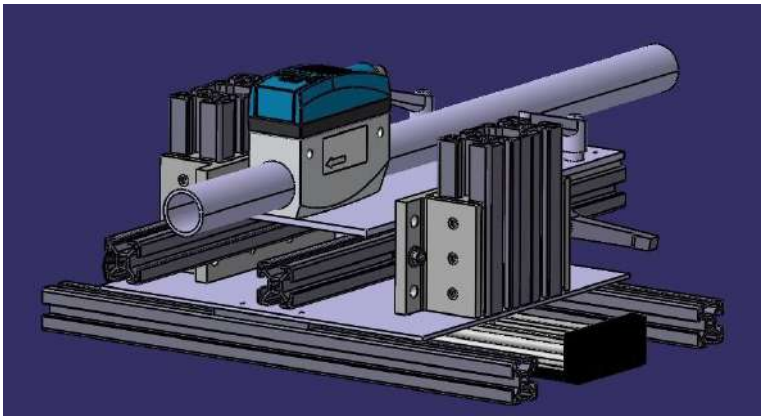

Figure 11: Theoretical structure displaying the adjustment fixation for the wind tunnel. The nozzle is not shown, neither is the pressure sensor

4.2 The nozzles

The nozzles used in the wind tunnel were produced in order to fit the fixation shown in Figure 9. They have been all produced (unless otherwise specified) in an axisymmetric way, using the characteristics method produced by [2]. The design Mach number was changed depending on the nozzles, and the throat diameter changed from nozzle to nozzle. Changing the throat diameter allowed to change the mass flow rate through the nozzle, due to Equation 1. All the nozzles have been designed, unless otherwise specified, using a heat capacity ratio (γ) of 1.4. The convergent part was not created following a specific method; it was designed by intuition creating smooth walls. One example of a nozzle cross-section is shown in Figure 12

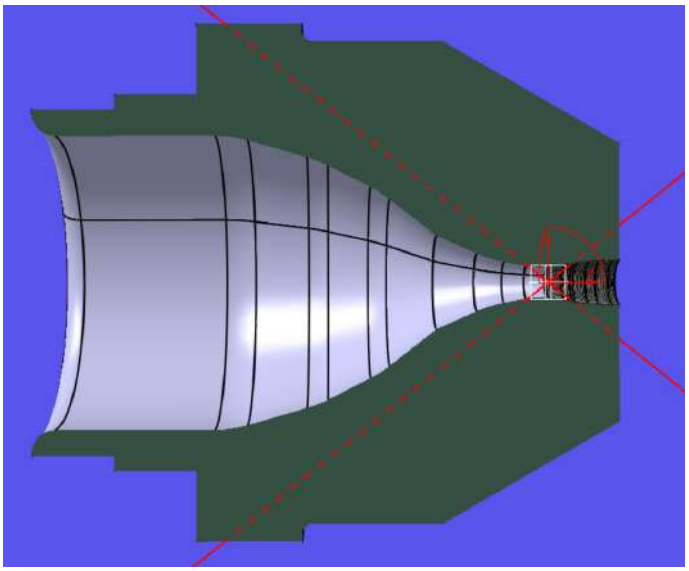

Figure 12: Cross-cut of Nozzle_V0 (designed for Mach 2.2 at the outlet, with a throat diameter of 2.5mm)

The complete list of all the nozzles built is shown below:

- Nozzle_V0: has throat diameter of 2.5mm, and is made for Mach 2.2
- Nozzle_V1: has throat diameter of 1mm, and is made for Mach 2.2. It also has a downstream structure for mach lines and shock visualization
- Nozzle_V2: has throat diameter of 2mm, and has no structure downstream. It has a 2mm constant section part after the nozzle. It is made for Mach 2.2
- Nozzle_V3: has throat diameter of 2mm, and no structure downstream. It has a 2mm constant section part after the nozzle. It is made for Mach 2

- Nozzle_V1modif: same as Nozzle_V1, but the downstream structure has been removed using a hacksaw
- Nozzle_V4: has a throat diameter of 2mm, and has no structure downstream. It has a 1mm constant section part after the nozzle. It is made for Mach 1.4

4.3 The Schlieren observation system

This part details the Schlieren system used to observe the flow. We also detailed the planned new system.

4.3.1 The Schlieren and Shadowgraphy visualization techniques

In order to visualize the flow, we have access to a lens assembly as shown in Figure 4. Such assembly will allow us to visualize the flow either in Shadowgraphy, or in Schlieren technique. While the technical difference between the two techniques is minimal (we only add a razor blade for the Schlieren assembly), the imaging results are quite different. In fact, as explained in [4], the Schlieren method shows light according to $\frac{\partial \rho}{\partial x}$, while the Shadowgraphy technique shows light according to $\frac{\partial^2 \rho}{\partial x^2}$. Better understanding can be obtained via Figure 13.

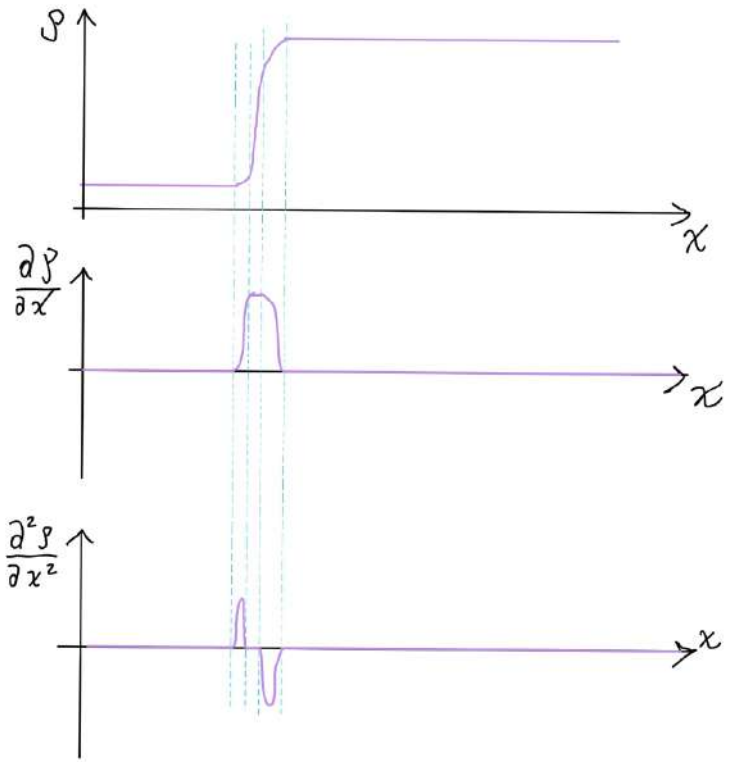

Figure 13: Evolution of the density, first and second derivatives of the density along x. In the scheme, we can suppose the presence of a shockwave along x (increase in density). When using the Schlieren technique, we should see light according to $\frac{\partial \rho}{\partial x}$, thus only one bright line. On the other hand, when using the Shadowgraphy technique, we will see light according to $\frac{\partial^2 \rho}{\partial x^2}$, thus we will first observe one light line, then a dark line.

Another example of the Schlieren vs Shadowgraphy techniques is shown in Figure 14.

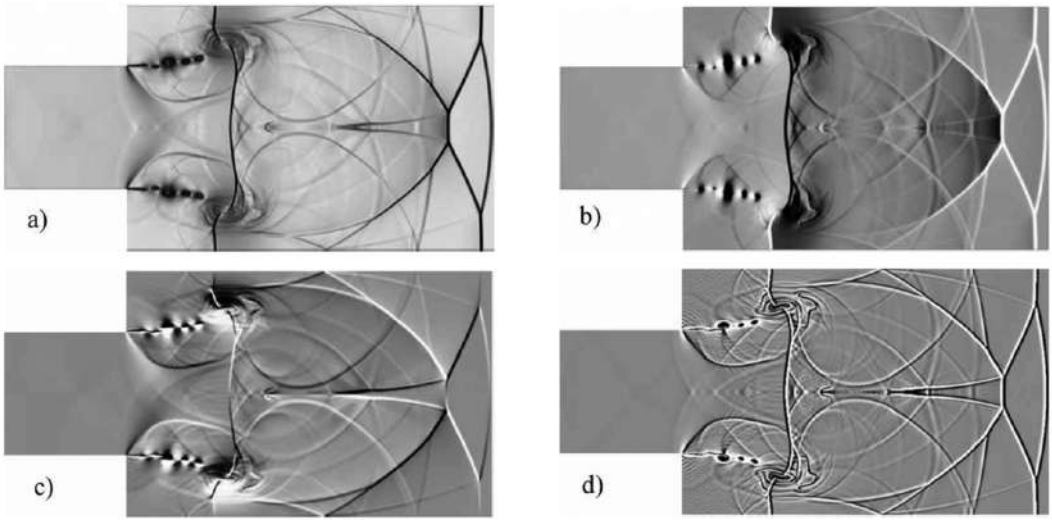

Figure 14: Images from a numerical solution of a supersonic jet-exit flowfield, rendered as (a) bright-field schlieren, (b) vertical-knifeedge schlieren, (c) horizontal-knife-edge schlieren, and (d) shadowgraphy, from [10]

Note that for the Schlieren assembly, the position of the razor blade (vertical or horizontal) has an influence on the result seen.

4.3.2 The Schlieren alignment procedure

The Schlieren system used for the moment will be the same of the old wind tunnel (for simplicity). The system, however, needs to be aligned properly before use. To explain the alignment procedure, we will refer to Figure 15

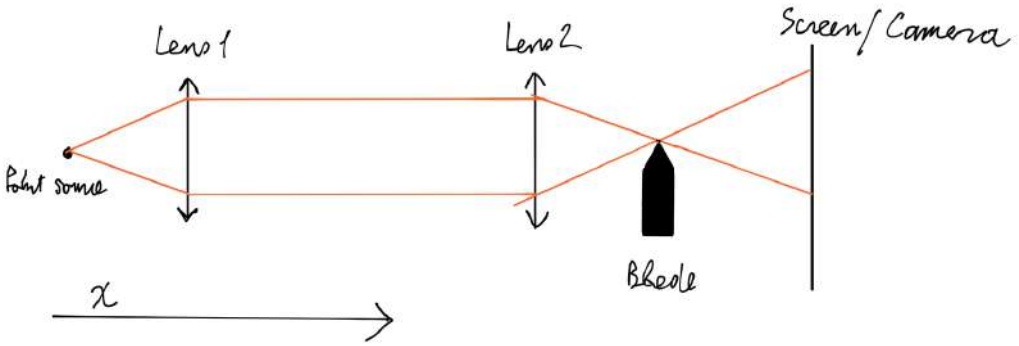

Figure 15: Scheme of a Schlieren assembly, lens based (a mirror-based option is also possible)

To align the system:

1. one must first position the first lens such that the light beam between the first lens and the second lens is straight (neither converging nor diverging). In theory, this is done by placing the point source at a focal length distance from the first lens. However, irregularities can lead to errors, so it is better to check the positioning by using a piece of paper right after the first lens, measure the diameter of the beam at that location, then make sure that the diameter is the same just before the second lens. If the beam became larger when approaching the second lens, the first lens must be moved towards positive x. If the beam is converging, the first lens will need to be pulled towards negative x.
2. Once a straight beam has been created between the first and the second lens (test section), we have to make sure that the beam is centered with the second lens. This implies centering the beam inside the second lens by moving the second lens
3. As long as the razor blade is not blocking the light path, a circular image will be projected on the screen. The disc shown can have blue edges at some locations of the circle. This means that the first lens is not exactly coaxial with the light source, thus adjust the first lens in height and lateral position, then repeat step 2

4. The second lens will focus the beam at a point. The goal is to position the blade such that half of the focus point is covered by the blade edge, and half is not.

5. Positioning a screen after the blade will make visualization of the flow possible. Note that the image on the screen will be reversed

Concerning the position of the razor blade, a few tips will help. Ater discussing with Teaching Assistant Lionel Bleich, a positioning protocol for the razor blade could be established:

- First, the razor blade should be positioned approximately at the focus of the light rays
- Then, it must be raised until the figure displayed by the camera is top orange, bottom blue (see Figure 22)
- Finally, the blade must be moved slightly along the x direction (see Figure 15) until the light level is uniform across the picture. Switching the camera visualization to Black and White can ease that procedure

A general rule when performing those kind of manipulations, is to pay attention to the exposure of the camera. We must avoid overexposure at all costs (if the camera is expensive, there is the risk to damage the sensor). Overexposure can happen fast, for example by moving the razor blade we might open completely the path of the lightbeam.

4.3.3 The Schlieren focus problem

It was also found that, even though in theory, the whole region between Lens 1 and Lens 2 could be used for testing, in practice, only a portion of that space ended up being in focus when viewed from the camera. By changing the various settings of the system, we ended up realizing that the size of the orifice creating the punctual light source had an influence on such focus zone[3]. For the moment, the possible sizes of screen holes are 100 and 500 μm. We took 3 pictures (using the Nikon D850 camera and the Nikon ED AF MICRO NIKKOR 20mm 1:4D objective) of the point of a toothpick in the test zone (between the two lenses): one just after Lens 1, the other in the theoretical focus zone, and the other just before Lens 2. An image of the setup is shown in Figure 16

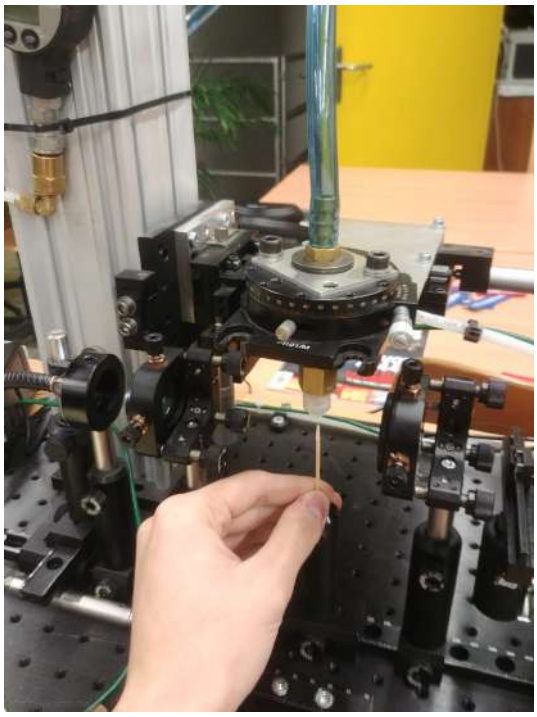

Figure 16: Setup used to check the influence of the hole size on the focus zone

All the images were taken for the 100 and for the 500 μm hole. The pictures are shown in Figures 17 and 18.

[3]The punctual light source is created by placing a normal light source behind a screen with a small hole

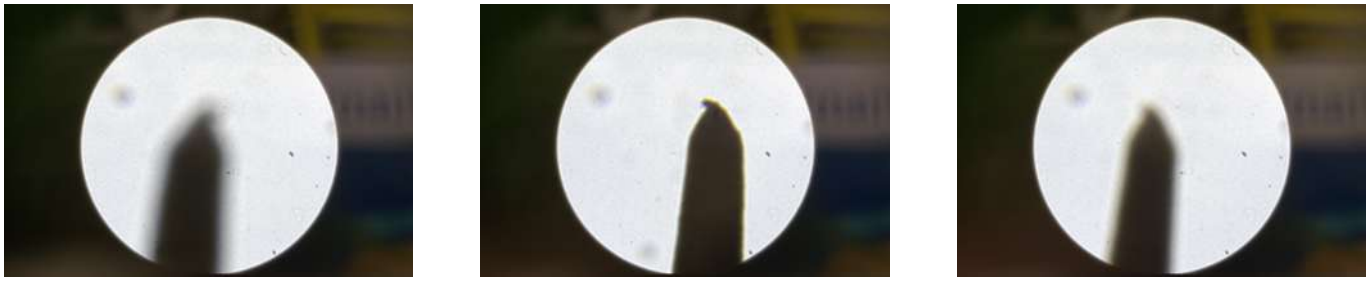

(a) Toothpick after Lens 1 (b) Toothpick in the focus zone (c) Toothpick in front of Lens 2

Figure 17: Images obtained using the 500 μm hole

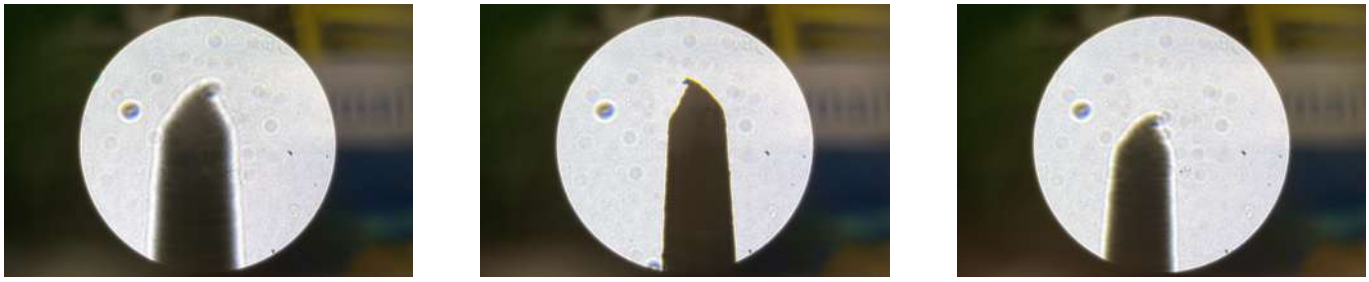

(a) Toothpick after Lens 1 (b) Toothpick in the focus zone (c) Toothpick in front of Lens 2

Figure 18: Images obtained using the 100 μm hole

As can be seen from Figures 17 and 18, the 100 μm hole allows for better image sharpness along the whole test region. However, using a smaller hole also leads to less light available for the system (25 times less in that case). Also, using a smaller hole makes it easier to identify non-homogeneities in the original light source[4]

4.4 Example image

Now that a comprehension of the behaviour of the Schlieren/Shadowgraphy system has been obtained, we can make an example image using the setup of Figure 4. The image has been obtained using a 500 μm pinhole (small hole creating an approximately punctual source), 25mm lenses and a razorblade. We used the Nikon camera system (Nikon D850+Nikon ED AF MICRO NIKKOR 20mm 1:4D). The idea was to display the flow impacting the edge of a pipe, as shown in Figure 22

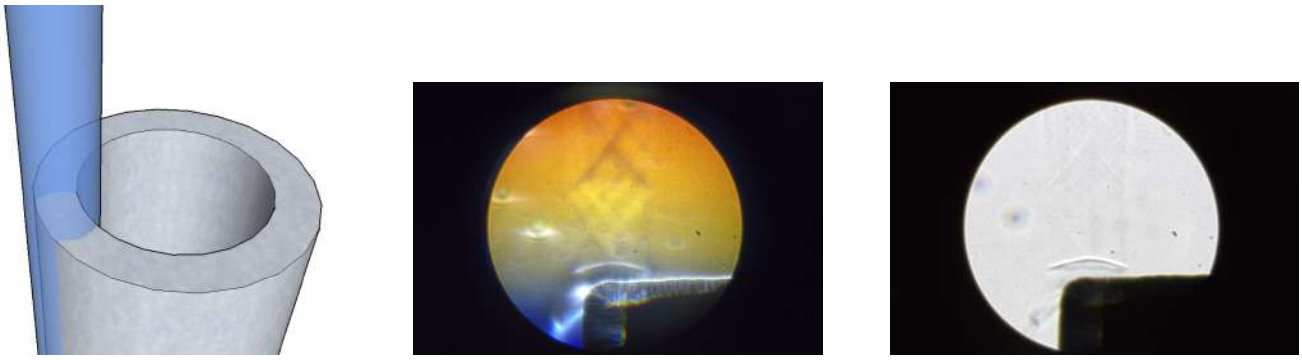

(a) Scheme of the experiment (b) Schlieren image (c) Shadowgraphy image

Figure 19: Example of the same image, taken with both the Schlieren method, and the Shadowgraphy method. The image shows an air jet impacting the pipe (6mm diameter)

[4]the lightsource behind the screen with the hole is composed of an array of LED's, creating light that is then converged on optical fibers. The light is hence not 100% uniform; the spaces between 2 LED's produce less light than the center of a LED.

Note how the shockwaves coming from the supersonic jet are shown in one grey color on the Schlieren image, while they are shown by two light and dark lines on the Shadowgraphy image.

4.4.1 List of components

While during most of the project, the setup shown in Figure 4 was used, the idea would be to create two separate wind tunnel benches; one linked to the compressed air system (the didactic, previous one), and one made for the JAG-7 compressor. For the latter to appear, a second observation system must be produced. Such system can be created using the components of Table 1.

Object and link	**Total quantity (already available)**
Camera bracket	1
Metric rail, 600mm	1
Rail clamp, 50mm	4
Metric rail, 70mm	2 (1)
Rail clamp, 25.4mm	4
75mm internal column (pack of 5)	1
75mm external column (pack of 5)	1
100mm internal columns	2 (1)
100mm external column	2 (1)
Optical supports	2
Pinhole mount	2
25mm lenses	2
50 μm pinhole	1
100 μm pinhole	1
XYZ stage for the razor blade stage	1
M6 cube to support the XYZ stage	1
Base threaded aluminium plate	1
50mm external column	1(1)
50mm internal column	1 (1)
Camera post washer	1 (1)
Camera post clamp	1 (1)
Camera post	1 (1)
Lamp	1 (1)

Table 1: Components needed for the new Schlieren assembly. The components already available at the lab are in brackets (for example, we do not need to buy the lamp)

Once we assemble all the components of the system, we are able to obtain a test table similar to the previous one (the older from Figure 4), being shown in Figure 20

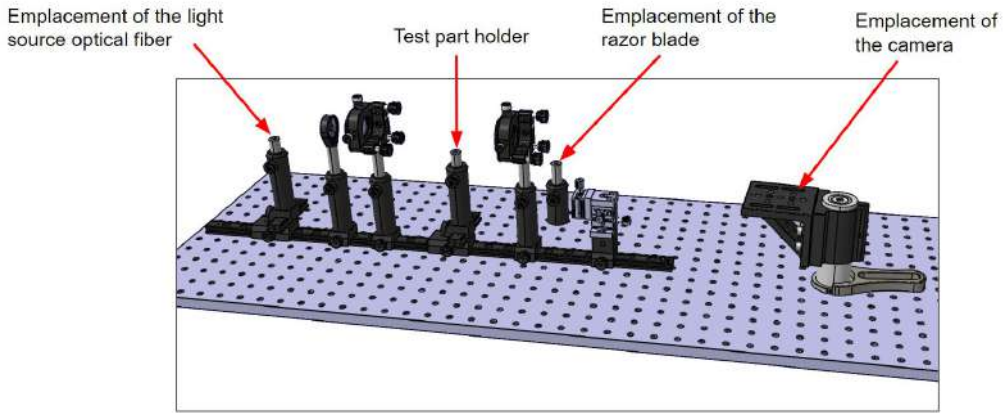

Figure 20: Image showing the new schlieren system, as planned. The camera, test piece and light source are not shown. The bracket holding the lightsource, and the bracket holding the razor blade are not shown. Those elements could be 3D printed, once all the components are received.

5 The various experimentations

Now that we have the theoretical knowledge, as well as the hardware needed for the wind tunnel we can proceed with various tests:

5.1 Experimentation 1

On Week 7, a first attempt to display the the flow at the exit of the new nozzle was performed. To do so, we built the setup of Figure 21.

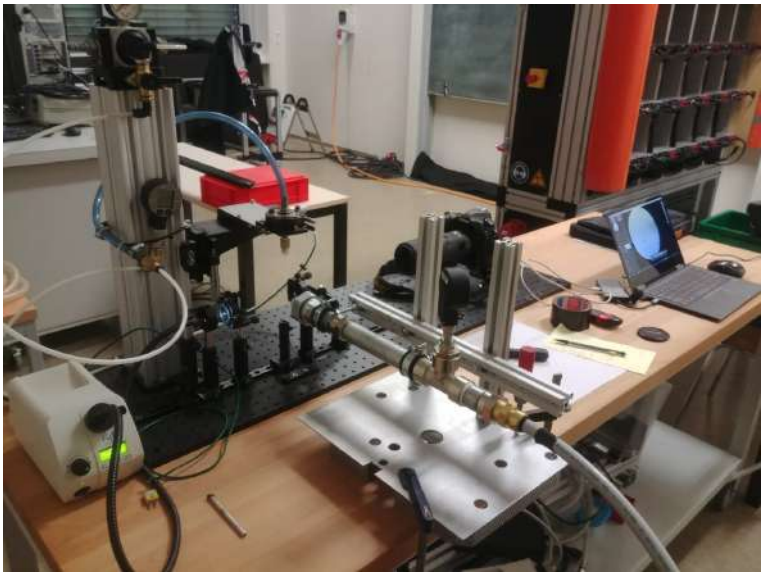

Figure 21: Setup used to test the new Mach 2.2 nozzles, coupled with the JAG-7 270E compressor

After building the setup, we were able to observe the flow using the previous Schlieren assembly, using a 500 μm pinhole and 25mm lenses. The Nikon camera system (Nikon D850+Nikon ED AF MICRO NIKKOR 20mm 1:4D) was used. The following images were obtained for two pressure levels: one low pressure, and one higher pressure. For simplcity, no pressure regulator was installed just before the wind tunnel. We instead relied on the pressure regulator already mounted at the outlet of the compressor.

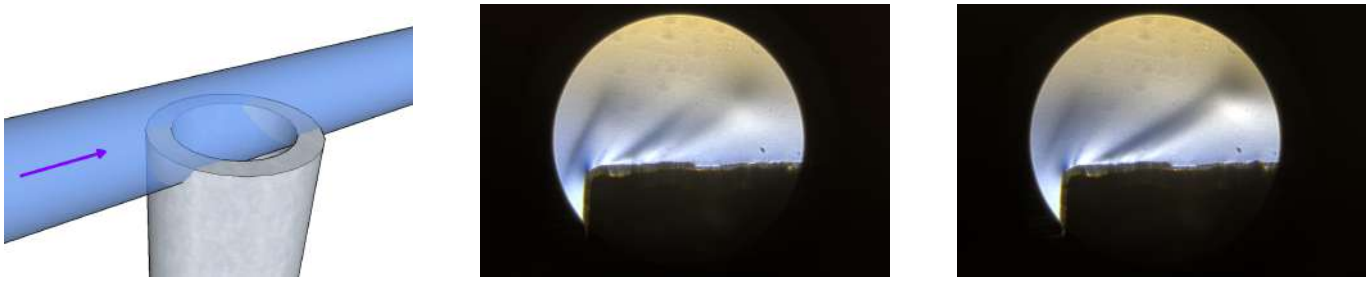

(a) Scheme of the experiment (b) Low pressure (c) Higher pressure

Figure 22

We notice more sloped Mach/Shock waves for a higher pressure (coherent with the theory). During this first experimentation, we also came across a list of problems:

- Small visualized area
- Non-constant compressor pressure (ended up stabilizing at 7.30 bar absolute pressure)
- Improvable imaging

More tests must be performed, in order to evaluate the capacities of the setup

5.2 Experimentation 2

The second experimentation's goal was to establish the working of the nozzle on a clear way. In fact, after Experimentation 1, we had no idea if the nozzle actually performed as supposed to. The idea behind Experimentation 2 is that observing the shock waves and Mack lines would allow us to determine in which operation regime the flow is. The operation points of the nozzle can be determined by the phenomena seen in the flow. For more details, refer to Figure 23

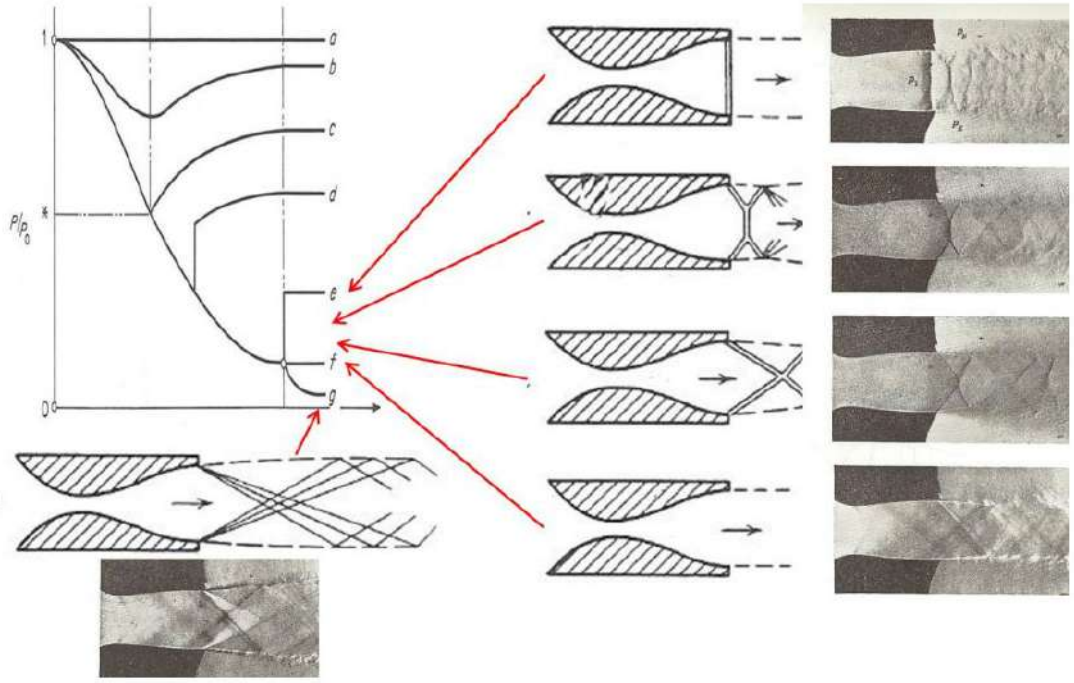

Figure 23: Figure from [4]: Various phenomena visible at the end of a nozzle. In the over-expanded flow (d,e) we can observe first an oblique shock wave, then diamond structures. In the optimal case (f) we do not observe anything except Mach waves, while Prandtl-Meyer fans, followed by diamond structures are seen in under-expanded flows (g). P represent the static pressure of the flow.

The experimentation was carried over using the same identical setup as Figure 21, without the metal tube in the way of the air jet. 25mm lenses were used. We also centered the flow in the view vield, and set-up the Schlieren/Shadowgraphy assembly the best way we could. We also placed the jet in the most focused position possible between the two lenses. We carried over various tests for various pressures, and viewed the flow. Unfortunately, the tests were done only with the pressure sensor and not with the flowmeter. Having that flowmeter would have allowed us to access informations about flow, but also pressure[5] and temperature.

During the tests, we first opened the valve, thus letting air escape through the nozzle, then we regulated the pressure output on the pressure regulator to match the wanted pressure[6]. We also reported the static pressure from the pressure sensor.

The results of the experiment are summed up in Figure 24

[5]the manufacturer does not specify if the pressure measured is the static or the total pressure

[6]the pressure from the pressure regulator is a relative pressure. It is unknown whether it is a total or a static pressure

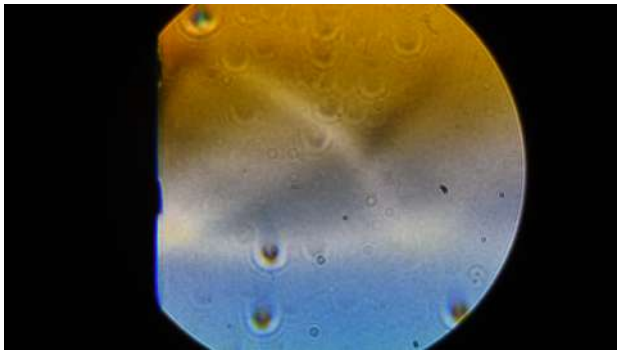

(a) 4 bar, Schlieren

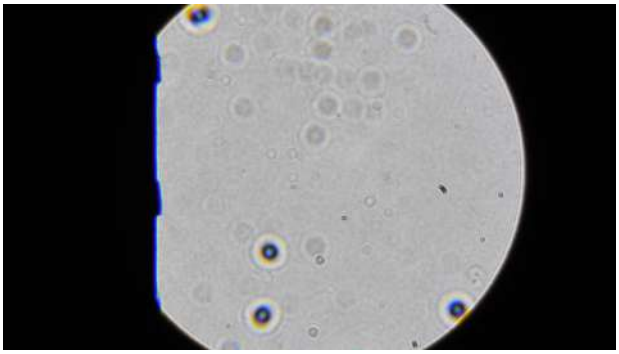

(b) 4 bar, Shadowgraphy

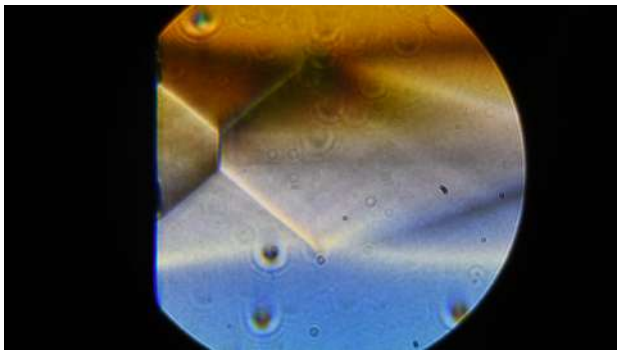

(c) 6 bar, Schlieren

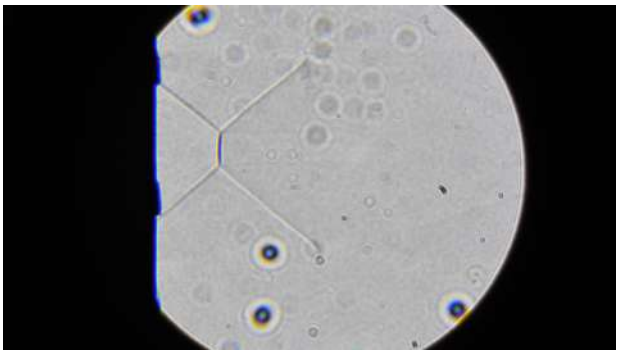

(d) 6 bar, Shadowgraphy

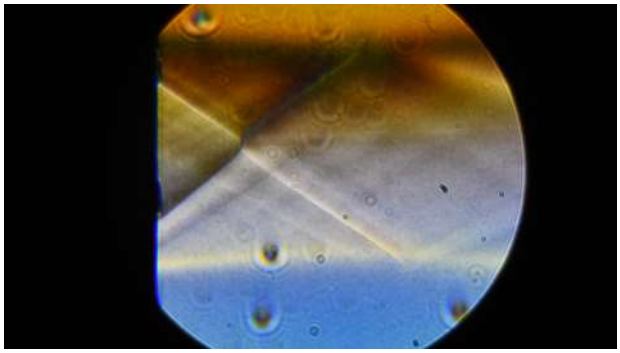

(e) 8 bar, Schlieren

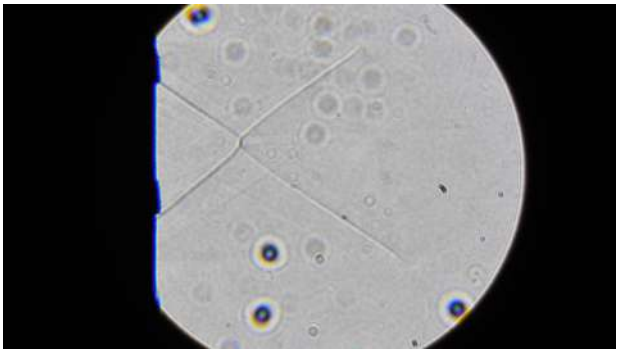

(f) 8 bar, Shadowgraphy

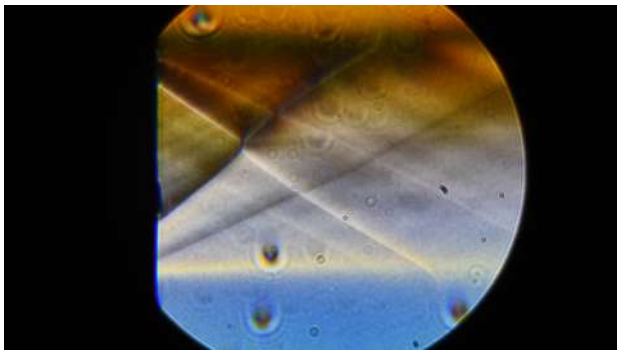

(g) 10 bar, Schlieren

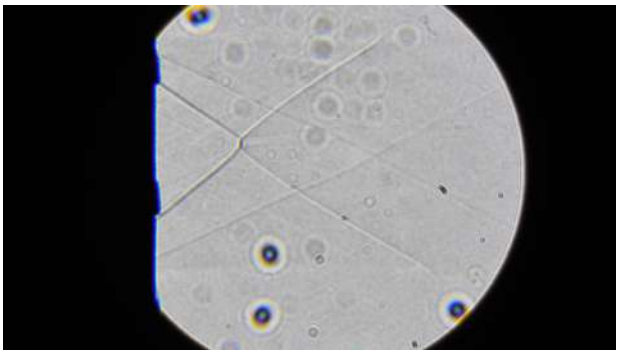

(h) 10 bar, Shadowgraphy

Figure 24: Imagery from Experiment 2. Each image was taken for a certain pressure, measured at the pressure regulator: 4,6,8 and 10 bars (relative pressure). We also measured the static absolute pressure using the pressure sensor: 4.56, 6.67, 8.75 and 11.05 bar. The ambient pressure was 0.96 bar. The more the compressor pressure was elevated, the less stable over time the pressure was.

From Figure 24 we have that the Mach number evolves from around 1.8 (at 8 bars) to 2.2-2.4 at 10bars. During the experiment, one quick test was done at the maximum allowable pressure by the compressor, leading to Mach of

2.7. The Mach numbers were measured using the slopes of the Mach lines, so large errors can be found.

This experiment has shown that the current system is able to produce speeds around Mach 2.2 (unexpected, due to the nozzle being made for Mach 2.2), but we are not able to reach for a nominal operation point. We also notice a structure composed of what looks like a conical shock wave, with constant slope at the outlet of the nozzle. we have to investigate on what it is.

5.3 Experimentation 3

After testing the Nozzle_V0, we decided to test a nozzle that could allow us to directly visualize some shock waves/phenomena without having to add anything outside from the nozzle. Hence, we decided to create Nozzle_V1 as shown in Figure 25

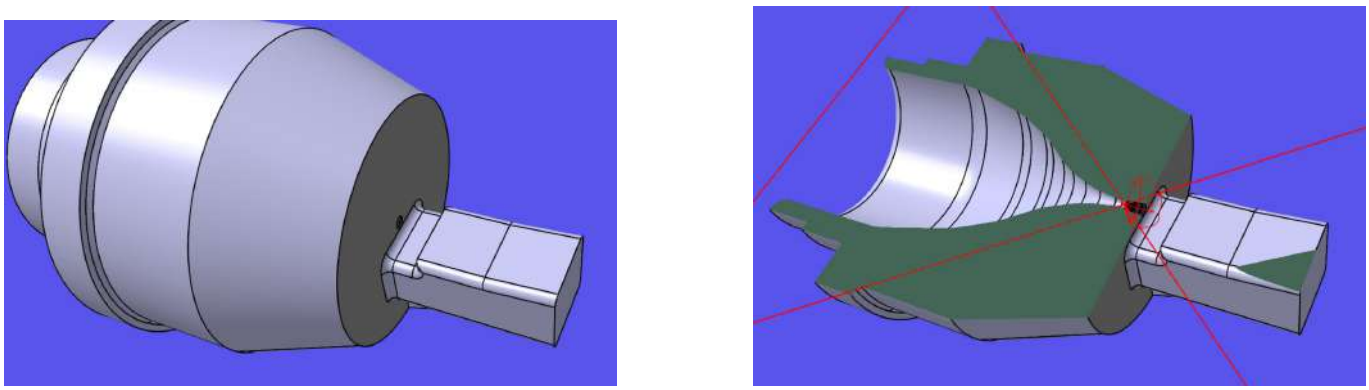

(a) external view of Nozzle_V1

(b) cross-cut of Nozzle_V1

Figure 25: Nozzle_V1, the nozzle used for Experimentation 3. The nozzle has a first obstacle slightly facing the nozzle, parallel to the flow. Then, an upward slope of 4 degrees has been produced

We tested the nozzle using the same method as Experimentation 2. Still, 50mm lenses were used in the system instead of 25mm ones. The results are only provided in Schlieren observation, and can be seen in Figure 26

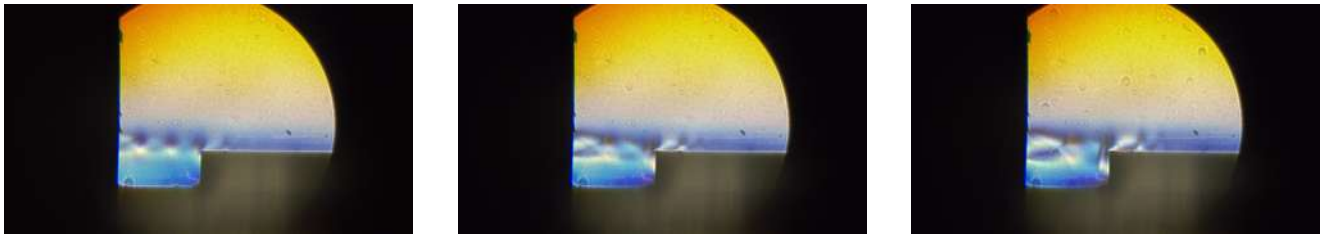

(a) Reservoir pressure: 4 bar (relative), static: 4.57 bar (absolute)

(b) Reservoir pressure: 6 bar, static: 6.65 bar

(c) Reservoir pressure: 8 bar, static: 8.78 bar

(d) Reservoir pressure: 10 bar, static: 11.06 bar

(e) Reservoir pressure: maximum (12.7) bar, static: 13.6 bar

Figure 26: Imaging obtained when performing Experimentation 3, for various pressure levels. The Static and reservoir pressure, under the method detailed in Experimentation 2 are provided for each image

After the experiments, we realized a few things, first of which being the fact that the 50mm lenses got dirtier the more the experiment was carried on. This can be seen because residues are scarce in the 4bar image, and numerous for the maximum pressure image. Next, we notice that the diamond formations downstream the nozzle have a rounded shape the more the pressure is increased. This could be explained by a phenomena called barrel shock. We also noticed that the whole jet has a tendency to deflect downwards when interacting with the downstream structure. On the other hand, the slight ramp of 4 degrees upwards downstream the flow generated no observable phenomena.

After the experiment, we decided to continue future tests only with the 25mm lenses because we do not need a view as vast as what is obtained with the 50mm ones. Also, we decided to increase the throat diameter to 2mm, and remove the downstream assembly. We also discussed whether adding a constant section segment just before the exit of the nozzle could help the flow or not. After doing the test, we had the idea to chop down the downstream structure to check just the exit flow from the nozzle. An image obtained for the maximum possible reservoir pressure (12.7 bar relative pressure) is provided in Figure 27

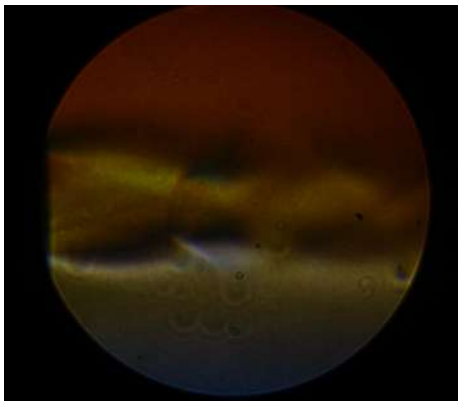

Figure 27: closeup view of the flow downstream Nozzle_V1, without downstream structure. The flow was observed with 25mm-lenses. We can clearly observe a barrel shock.

NOTE: while being an interesting phenomenon, barrel shocks are not suited for our application, ideally we need no shocks, just a clean unidirectional flow in order to use the jet to test various profiles.

5.4 Experimentation 4 and 5

Following the same procedure as Experiment 2, we tested Nozzle_V2. This nozzle has the particularity of having a throat of 2mm (against 2.5 for Nozzle_V0), is designed for Mach 2.2 and has a 2mm constant section segment after the nozzle obtained via characteristics method. The reduced throat section means a smaller air flow, this increasing the chances for the compressor to show all the possible operation regimes of the nozzle. Of course, ideally the test should be done with the flowmeter. The images obtained when testing the nozzle are provided in Figure 28

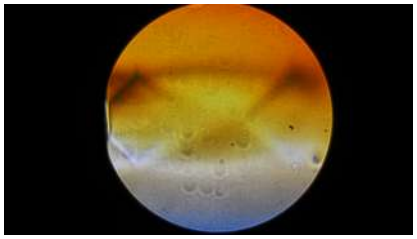

(a) Reservoir pressure: 4 bar (relative), static: 4.70-4.70 bar (absolute)

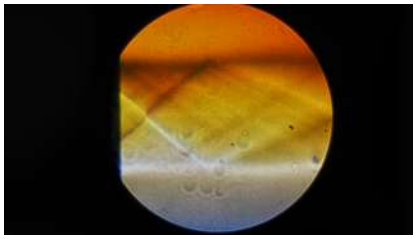

(b) Reservoir pressure: 6 bar, static: 6.77-6.77 bar

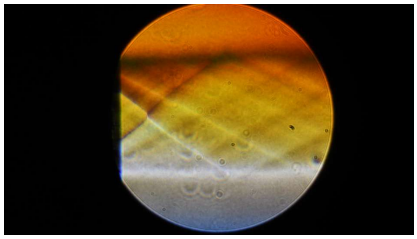

(c) Reservoir pressure: 8 bar, static: 8.94-8.93 bar

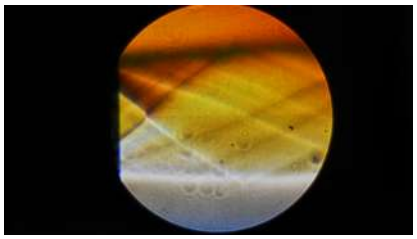

(d) Reservoir pressure: 10 bar, static: 11.07-11.06 bar

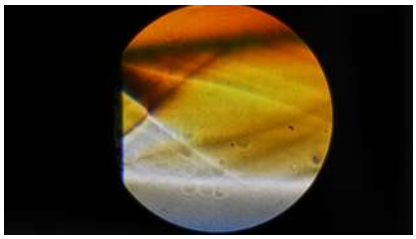

(e) Reservoir pressure: maximum (12.7) bar, static: 13.50-13.20 bar

Figure 28: Imaging obtained when performing Experimentation 4 (Nozzle_V2), for various pressure levels. The Static and reservoir pressure, under the method detailed in Experimentation 2 are provided for each image. We provided two pressure levels for the static pressure: one taken at the moment of the image, the other 10 seconds later, in order to show pressure evolution with time, and deduce the behaviour of the compressor

Experimentation 3 consists in testing Nozzle_V3, which is identical to Nozzle_V2, except it is designed for Mach 2. The imaging of the experimentation is provided in Figure 29

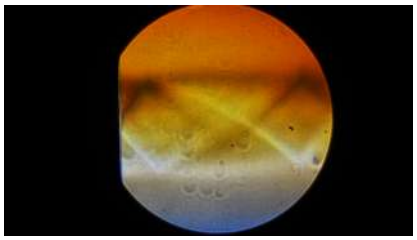

(a) Reservoir pressure: 4 bar (relative), static: 4.58-4.58 bar (absolute)

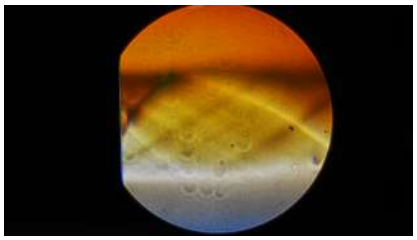

(b) Reservoir pressure: 6 bar, static: 6.74-6.74 bar

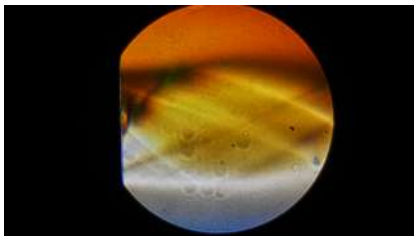

(c) Reservoir pressure: 8 bar, static: 8.83-8.82 bar

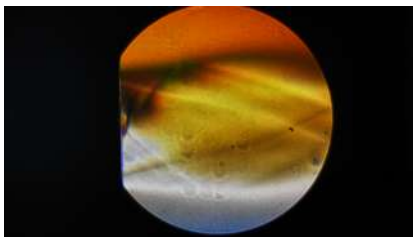

(d) Reservoir pressure: 10 bar, static: 11.05-11.02 bar

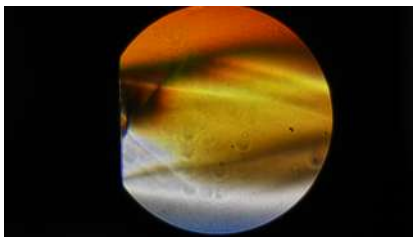

(e) Reservoir pressure: maximum (12.7) bar, static: 13.52-13.09 bar

Figure 29: Imaging obtained when performing Experimentation 5 (Nozzle_V3), for various pressure levels. The Static and reservoir pressure, under the method detailed in Experimentation 2 are provided for each image. We provided two pressure levels for the static pressure: one taken at the moment of the image, the other 10 seconds later, in order to show pressure evolution with time, and deduce the behaviour of the compressor

After the experiments, we realize that, unlike Experimentation 1, we are able to obtain some Prandtl-Meyer fans directly downstream the nozzle, which can be seen by the fact that the jet becomes wider. Also, diamond-like structures form at that point behind the nozzle. We can hypotise the appearance of PM fans after the nozzle, by the fact that, maybe the flow rate is acceptable by the compressor, without too big pressure drops; however to proove that, we should test again Nozzle_V0 and Nozzle_V2 or V3, with the flowmeter. We still see the shock-like cone just after the nozzle, except it is probably starting 2mm inside the nozzle, because of the 2mm constant section segment. The current hypothesis allowing to explain that "shock cone" is that it is actually a strong Mach line (notice the different slope between Nozzle_V2 and Nozzle_V3). We can verify this hypothesis by building a new nozzle, and paying very high attention to the flow perturbators in the diverging side (printing it with a $25\mu m$ layer height, and smoothing in the CAD file all the edges). Unfortunately, it was not possible to launch this kind of impression due to printer calibration issues. So, instead, an idea was to build a nozzle dimensioned for Mach 1.4 and try to see if for Mach numbers lower than 2.2 the same Mach line could appear or not just after the nozzle.

5.5 Experimentation 6

The following experimentation was done on Nozzle_V4, built for Mach 1.4, a throat diameter of 2mm and a constant section length after the nozzle of 1mm. The idea was to see if similar strong Mach lines could be seen at the exit of the nozzle. The experimentation was done the same way as the others. Initially, the local was at an atmospheric pressure of 0.96 bar, the compressor was loaded around 12.4 bar (relative). Obtained images are shown in Figure 30

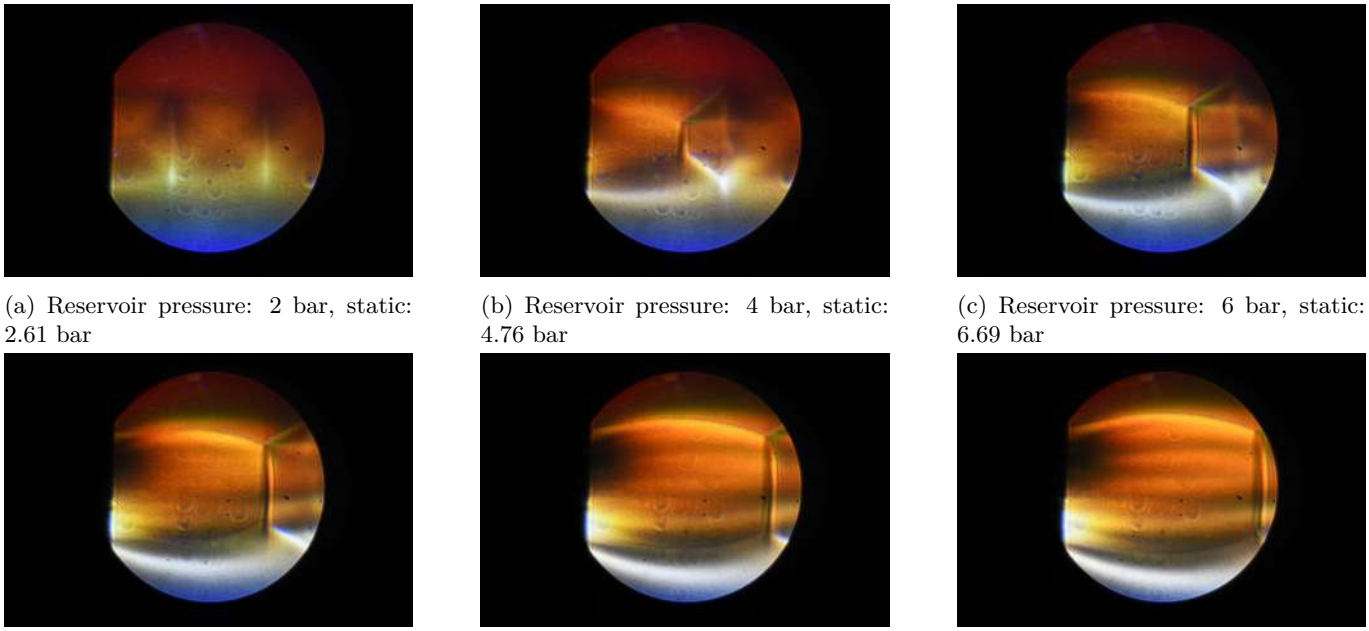

(a) Reservoir pressure: 2 bar, static: 2.61 bar

(b) Reservoir pressure: 4 bar, static: 4.76 bar

(c) Reservoir pressure: 6 bar, static: 6.69 bar

(d) Reservoir pressure: 8 bar, static: 8.81 bar

(e) Reservoir pressure: 10 bar, static: 11.01 bar

(f) Reservoir pressure: maximum, static: 12.36 bar

Figure 30: Exit flow from Nozzle_V4

Concerning the analysis of the flow, we notice the appearance of a barrel shock, increasing in size the more the reservoir pressure grows. Also, we do not see any strong Mach line at the end of the nozzle. The test is inconclusive.

5.6 Experimentation 7

Before finishing the project, one last concern would be the reproducibility of the experiments, more precisely, if various nozzles built with the same machine may have differences in performance. To do so, we used the two Nozzle_V0 produced initially, and checked if they had the same performance. Figure 31 shows the results for each nozzle

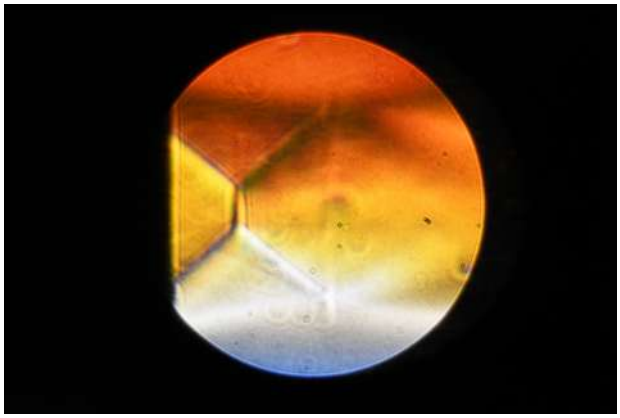

(a) Reservoir pressure: 6 bar, First nozzle

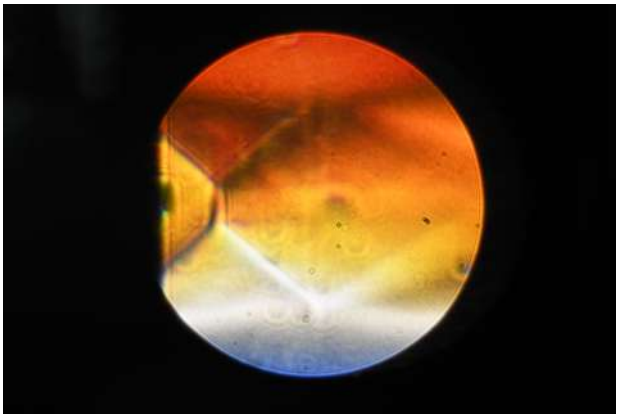

(b) Reservoir pressure: 6 bar, Second nozzle

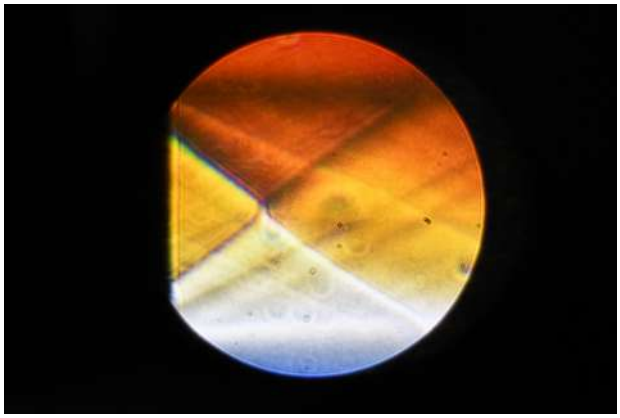

(c) Reservoir pressure: 10 bar, First nozzle

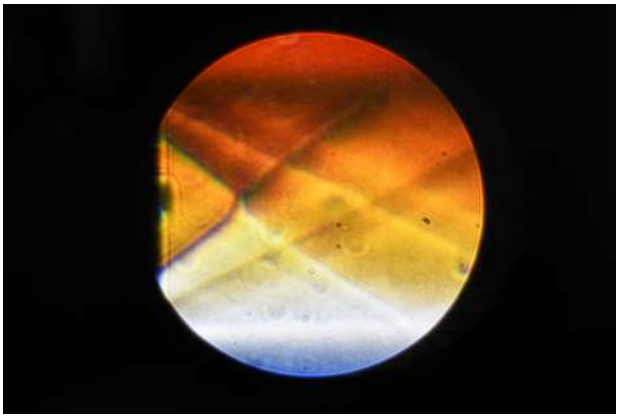

(d) Reservoir pressure: 10 bar, Second nozzle

Figure 31: Flow downstream two Nozzle_V0 nozzles

We notice from Figure 31 that the flow behind the nozzles are comparable. They are not 100% identical due to unique imperfections on each nozzle, but they are very similar. When doing the experimentation, we noticed some axial irregularities (differences when rotating the nozzle along its axis). Those problems are explained by the observations of the nozzles with the microscope.

5.7 Practical problems

During the various experiments, we realized that rusty water was accumulating in the purge tank of the JAG-7-270 E compressor. The main hypothesis is that water accumulates in the tank when the compressor is not used, thus makes the steel composing the tank rusty. The problem has been communicated to Volkart SA. The company answered (to Pietro DAVI), that "no worries are to be made, the color comes either from the oil or the machining residues".

Other practical problems could be the classical difficulty of aligning correctly the schlieren assembly, or the various leaks across the whole system.

5.8 Nozzle measurements

Concerning the measurement of the nozzles, the idea was to use a microscope in order to check if the nozzles printed were actually of the good dimensions. Those measurements were taken for all the nozzles using the microscope setup shown in Figure 32.

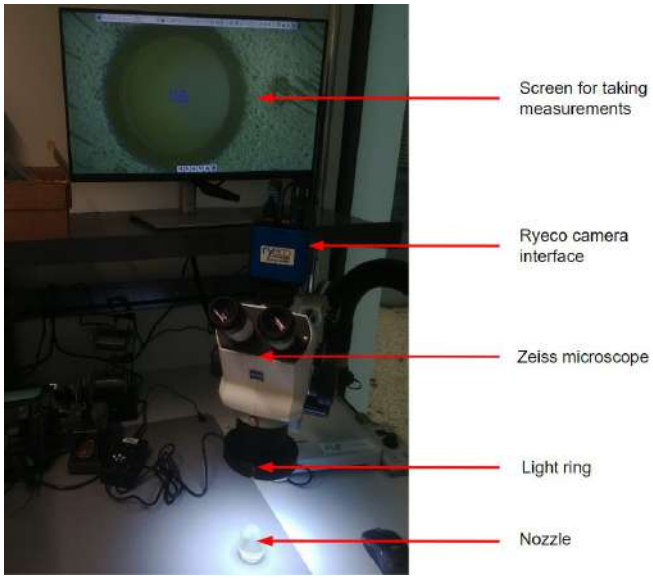

Figure 32: Setup used to take measurements of the nozzles. The setup is located at EPFL, at the SPOT building.

Using the microscope setup shown in Figure 32, we were able to measure the throat diameter of each nozzle. Those were compared with the theoretical diameters from the CAD files of each nozzle. Each measurement was taken 3 times then averaged. The data is shown in Table 2.

Nozzle	**Throat diameter [mm]**	**Theoretical throat diameter [mm]**
Nozzle_V0	2.527	2.5
Nozzle_V0	2.550	2.5
Nozzle_V1	0.963	1
Nozzle_V2	2.017	2
Nozzle_V3	2.017	2
Nozzle_V4	2.047	2

Table 2: Measurements of the throat diameter of each nozzle

The measurements of Table 2 have been produced using a three-points-circle tool on the Ryeco interface. During the measurement, we also measured the exit diameter of the nozzle, however, due to a mistake in the magnification used on the Ryeco interface, the informations obtained were not right. Still, observing the data from Table 2 we have that the dimensions of the nozzles are coherent with the CAD.

When observing the nozzles, we also came up with some unexpected problems, such as some imperfections on the nozzles. An example is shown in Figure 33.

Figure 33: Closeup view of Nozzle_V0, showing the presence of three support pins. Those pins were placed close to the nozzle on the Formslab slicer, however they were found to be in the way of the nozzle exit on the real nozzle.

5.9 Conclusion of the experiments

Some of the things that were understood after the series of experiments, is that a throat diameter of 2mm seems to provide acceptable results (bigger diameters lead to the difficulty of achieving nominal regime and beyond due to the limited flow of the compressor; while a smaller diameter like 1mm leads to the appearance of barrel shock waves.). Such diameter works well for Mach 2.2, but when lowering the mach number, barrel shocks can appear at high pressure. We noticed that the use of characteristics-based nozzle profiles resulted in no detachment of the flow at the throat. It is possible that using a different type of profiles could result in detachment.

When working with nozzles Nozzle_V0, Nozzle_V2 and Nozzle_V3, we noticed the appearance of strong mach waves at the exit of the nozzle. It is still unknown why those waves appear. Further testings must be pursued.

We also noticed imperfections on some nozzles (remains of support structures). Ideally, for next experimentations, observations at the microscope should be pursued before testing the nozzle.

Note: we did not actually test the compressor for various increasing values of throat area, as planned by the previous calculations. We direclty started with a value close to the maximum area allowed (2.5mm) and found out that even that was too big. However, potentially, there is spot for improvement between 2 and 2.5mm.

6 CFD study

During the project, some CFD studies have been performed, in order to check if the simulation was actually coherent with the reality, and also to gain CFD experience. We reported some outcomes of some simulations. Only successful simulations were reported. The software ANSYS Workbench was used. When not specified, default values have been used.

6.1 Simulation 1

Simulations 1's goal was to obtain the flow, for various reservoir pressure levels, for Nozzle_V2. So, the nozzle was loaded on CATIA V5, and we extracted the fluid volume, by supposing a 28.5mm diameter cylinder of air, 40mm long after the nozzle. See Figure 34

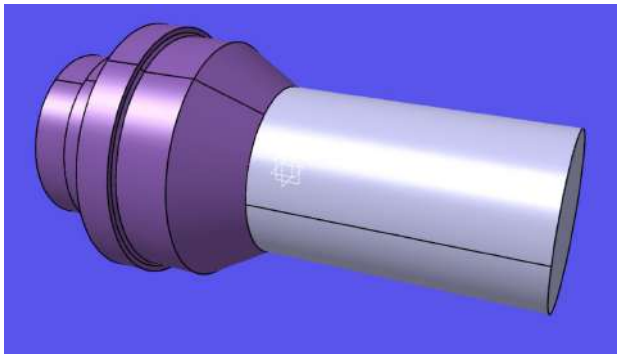

(a) Nozzle and fluid volume (note the 28.5x40mm downstream the nozzle)

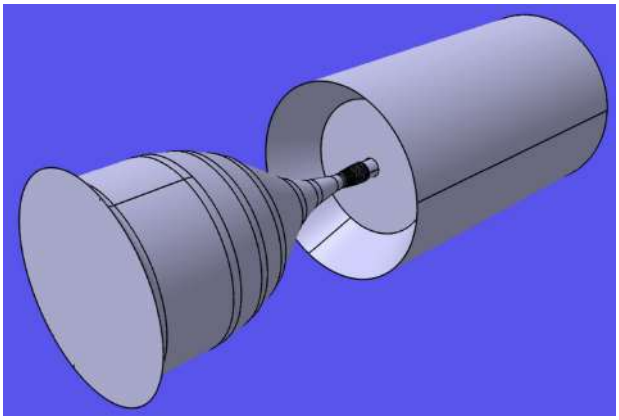

(b) Only the fluid volume around the nozzle

Figure 34: The CAD model used for the study

Once the CAD model was set, and then repaired (removing surfaces less than 0.06 mm thick), we set the inlet of the nozzle as a pressure inlet, the whole surface of the downstream cylinder (except the face facing the nozzle) as a pressure outlet, and every other surface as a wall.

The next step was to create a decent mesh for the system. The requirement was to have enough elements, especially in the critical regions such as the nozzle, and the downstream segment of the nozzle, without going beyond 500 000 elements for the Educational licence. We decided to use the Fluent meshing method, and perform the following operations:

- We set a Body Of Influence (7mm diameter cylinder, coaxial with the nozzle), inside the 28.5mm cylinder part of the fluid volume. We associated a 1.2 growth rate and a 0.3mm target mesh size to that BOI. The goal of that BOI is to refine the mesh in the outlet region, but only in the stream of the jet, in order not to waste elements, and to visualize diamond effects if present
- We set around the convergent-divergent part a face size of 0.2mm, and a growth rate of 1.1. The convergent section here only refers to the convergent close to the nozzle
- We set on the rest of the convergent, linking to the inlet, a face size of 0.8mm, growth rate of 1.1

The global surface mesh was generated using a growth rate of 1.1, minimum size of 8.59e-05m, maximum size of 1mm. We also generated 8 boundary layers, with a growth rate of 1.1, even though the simulation was planned to be done using the inviscid assumption. The mesh was finally generated with polyhedra elements, and was composed of 330 395 elements. The minimum orthogonality was 0.20 (widely sufficient), and maximum aspect ratio was 3.76. The mesh is shown in Figure 35

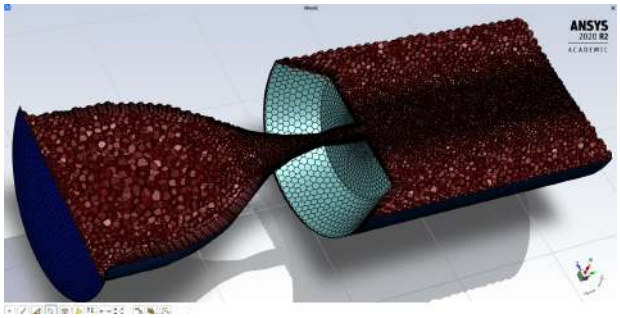

(a) Global view of the mesh

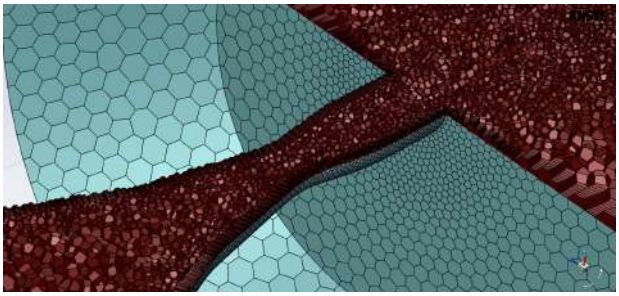

(b) Closeup view of the throat

Figure 35: Mesh used for Simulation 1. The mesh is cut along its length to show the internal elements. We see the polyhedra elements, as well as the 8 boundary layers

When solving, we used the following parameters:

- Density based solver, later changed to pressure based for stability issues

- Steady flow
- Operating conditions: 0 Pa
- Energy equation: on
- Heat exchanger: off
- Inviscid flow
- Material: Air, following the ideal gas law (1006.43 J/kg/K, 28.966 g/mol)
- Boundary conditions: 10, 8 or 6 bars at the inlet (absolute pressure), 1 bar at the outlet
- Standard solver

The conditions for convergence were residues less than 0.001 for all, except the continuity residue, needing 1e-6). After solving, we obtained the results shown in Figure 36.

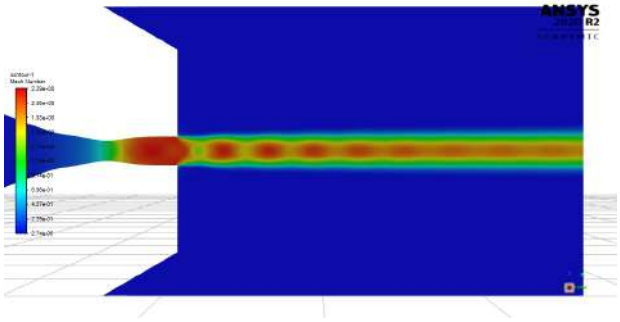

(a) 6 bar inlet, Mach number

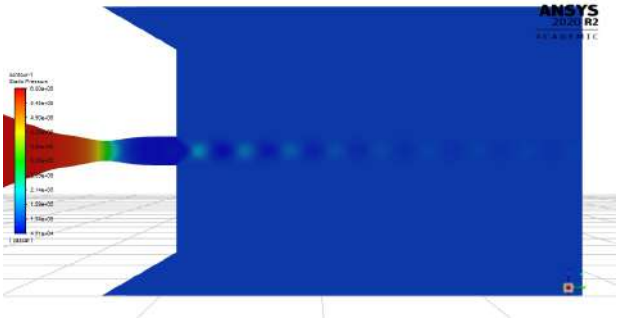

(b) 6 bar inlet, static pressure

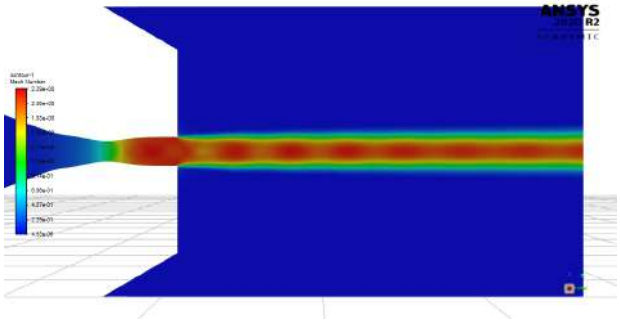

(c) 8 bar inlet, Mach number

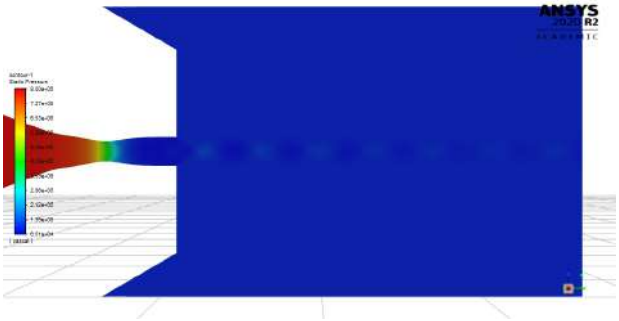

(d) 8 bar inlet, static pressure

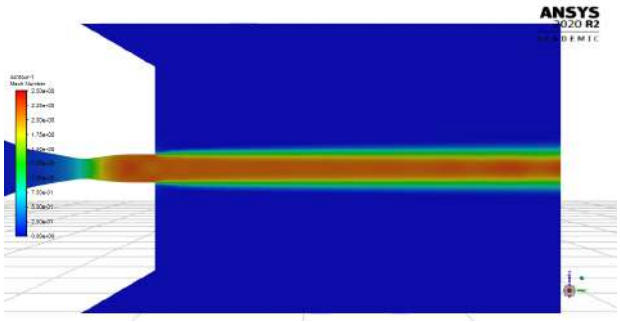

(e) 10 bar inlet, Mach number

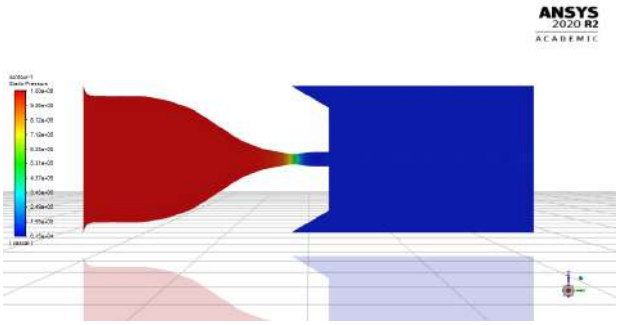

(f) 10 bar inlet, static pressure

Figure 36: Results from Simulation 1

Note that the simulations are not necessarily 100% correct. To ensure their trustmorthyness, we would have to perform a mesh convergence check, which can be hard because we may have to increase even more the number of elements in the mesh. Also, we would have to check if the results, and the various assumptions, are actually fulfilled.

If we consider the results correct, we will see that diamond structures disappear for a reservoir pressure of 10 bars (absolute), thus hinting the good working principle of the nozzle. As expected, the nozzle provides a Mach at 10 bars of approx. 2.2.

7 Conclusion and further works

At the end of this project we were able to produce a wind blower reaching Mach 2.2, with a throat of 2 and 2.5mm. We noticed no detached flow from our nozzles. Still, further studies need to be done concerning the following aspects:

- Is the data from the flowmeter and Schlieren imaging coherent with theoretical predictions?
- How can we include in a sealed way the thermocouple in order to have temperature informations[7]?
- Does nozzles created without the characteristics's method perform worse than current nozzles? What is the difference?
- The flowmeter and nozzle support structure (see Pietro DAVI's report), as well as the new Schlieren assembly must be bought and assembled
- Try nozzles with other printing precisions (smoother nozzles)
- Test elements downstream the blower in order to check if the interaction is what is expected (also compare with CFD if time allows)

It was found that with current compressor, it is hard to use nozzles with a throat larger than 2mm diameter in steady state at Mach 2.2, due to the too high mass flow rate. One possibility would be to empty the main tank directly through a nozzle, thus creating an instantaneous flow, lasting a few seconds, but having a way higher mass flow rate (solution adopted by [11]). The inconvenient is that such high flow rate won't be able to be measured by the flowmeter (over the maximum measurable flow).

Also, more studies must be conducted on the two not understood phenomena observed: barrel shocks, and more importantly, the conical structure just after the 2mm nozzles.

References

[1] Ansys Fluent | Fluid Simulation Software. URL: https://www.ansys.com/products/fluids/ansys-fluent.

[2] Axisymmetric Minimum Length Nozzle Design Tool. URL: https://www.mathworks.com/matlabcentral/fileexchange/85253-axisymmetric-minimum-length-nozzle-design-tool.

[3] Closed Return Wind Tunnel. URL: https://www.grc.nasa.gov/www/k-12/airplane/tuncret.html#:~:text=In%20the%20closed%20return%20tunnel,of%20the%20closed%20return%20tunnel.

[4] Compressible-fluid dynamics - EPFL. URL: https://edu.epfl.ch/coursebook/en/compressible-fluid-dynamics-ME-343.

[5] ECO 2 | Keller Pressure Sensor With Display -1-+30 bar 7/16" -20 UNF (Adapter G¼" in Scope of Supply). URL: https://www.distrelec.ch/en/pressure-sensor-with-display-30-bar-16-20-unf-adapter-in-scope-of-supply-keller-eco/p/30022452.

[6] FTMG-ISD25AXO | Débitmètre Sick FTMG pour Air, Hélium, Argon, Azote, Dioxyde de carbone, 14,7 l/min à 4417 L/min, raccord G1 mâle | RS. URL: https://fr.rs-online.com/web/p/debimetres/2101291.

[7] Numerical flow simulation - EPFL. URL: https://edu.epfl.ch/coursebook/fr/numerical-flow-simulation-ME-474.

[8] Open Return Wind Tunnel. URL: https://www.grc.nasa.gov/www/k-12/airplane/tunoret.html.

[9] Série JAG · Volkart Air comprimé SA. URL: http://www.volkart-sa.ch/fr/home/nos-produits/compresseurs-industriels/compresseurs-a-vis.

[7] positioning it on the pipes will lead to inaccurate data due to thermal diffusion

[10] A. Hadjadj and Alexey Kudryavtsev. Computation and visualization flow in high speed aerodynamics. *J. Turbul*, 6:33–81, 01 2005.

[11] Jay Pascual. Design of a supersonic wind tunnel. *Mechanical Engineering Undergraduate Honors Theses*, May 2007. URL: https://scholarworks.uark.edu/meeguht/21.

[12] Alan Pope and K. L. Goin. *High Speed Wind Tunnel Testing*. Wiley, January 1965. Google-Books-ID: yHF-TAAAAMAAJ.